Numerische Mathematik (2020) 144:157–200
https://doi.org/10.1007/s00211-019-01077-z

Numerische Mathematik

Computation of optimal transport on discrete metric measure spaces

Matthias Erbar[1] · **Martin Rumpf**[2] · **Bernhard Schmitzer**[3] · **Stefan Simon**[2]

Received: 21 July 2017 / Revised: 3 July 2019 / Published online: 24 October 2019

Abstract
In this paper we investigate the numerical approximation of an analogue of the Wasserstein distance for optimal transport on graphs that is defined via a discrete modification of the Benamou–Brenier formula. This approach involves the logarithmic mean of measure densities on adjacent nodes of the graph. For this model a variational time discretization of the probability densities on graph nodes and the momenta on graph edges is proposed. A robust descent algorithm for the action functional is derived, which in particular uses a proximal splitting with an edgewise nonlinear projection on the convex subgraph of the logarithmic mean. Thereby, suitable chosen slack variables avoid a global coupling of probability densities on all graph nodes in the projection step. For the time discrete action functional Γ-convergence to the time continuous action is established. Numerical results for a selection of test cases show qualitative and quantitative properties of the optimal transport on graphs. Finally, we use our algorithm to implement a JKO scheme for the gradient flow of the entropy in discrete transportation distance, which is known to coincide with underlying Markov semigroup, and test our results against a classical backward Euler discretization of this discrete heat flow.

Keywords Optimal transport on graphs · Proximal splitting · Gradient flows

Mathematics Subject Classification 65K10 · 49M29 · 49Q20 · 60J27

The authors thank Benedikt Wirth for a fruitful discussion concerning the decoupling with slack variables. Matthias Erbar, Martin Rumpf, and Stefan Simon have been supported by the *Deutsche Forschungsgemeinschaft* through the *Collaborative Research Centre 1060—The Mathematics of Emergent Effects* and the Hausdorff Center for Mathematics (Exzellenzcluster 2047).

✉ Stefan Simon
s6stsimo@uni-bonn.de

[1] Institute for Applied Mathematics, University of Bonn, Bonn, Germany

[2] Institute for Numerical Simulation, University of Bonn, Bonn, Germany

[3] Department of Mathematics, Technical University of Munich, Munich, Germany

1 Introduction

For a metric space $(\mathcal{X}, d)$ and a weighting exponent $p \in [1, \infty)$ optimal transport induces the p-Wasserstein distances W_p on the probability measures over $\mathcal{X}$. A remarkable property of Wasserstein distances is that they form a length space if the base space $(\mathcal{X}, d)$ is a length space, inducing the so-called displacement interpolation between probability measures [17]. The celebrated Benamou–Brenier formula for W_2 over $\mathbb{R}^n$ [3] can be interpreted as an explicit search for the shortest path between two probability measures. In the last two decades the geometry of metric spaces has extensively been studied by means of optimal transport. It has been observed that the 2-Wasserstein metric over probability densities in $\mathbb{R}^n$ formally resembles a Riemannian manifold [20] and that various diffusion-type equations can be interpreted as gradient flows for entropy-type functionals with respect to this metric [15]. For a comprehensive introduction we refer to the monographs [22,25].

Unfortunately, this rich geometry is not directly available when the base space $\mathcal{X}$ is discrete, since W_2 degenerates and does not admit geodesics. Maas [16] introduced a transport-type Riemannian metric $\mathcal{W}$ on probability measures over a discrete space $\mathcal{X}$ equipped with a reversible Markov kernel Q, based on an adaption of the Benamou–Brenier formula. A key ingredient in the construction is the choice of a *'mass averaging'* function θ that interpolates the amount of mass on neighbouring graph vertices. For the particular choice of θ being the logarithmic mean, the heat equation (with respect to the underlying Markov kernel) arises as gradient flow of the entropy with respect to this metric [16], yielding a discrete analogue of Otto's interpretation of diffusive PDEs. The same metric was independently introduced in [5] to obtain a spatial discretization of the Focker–Planck equation that retains a gradient flow structure and in [18] to interpret suitable reaction–diffusion systems as gradient flows. A generalization to non-linear evolution equations on discrete spaces is given in [10]. The notion of displacement convexity for this new metric is studied, for instance, in [6,19]. In analogy to the Lott–Sturm–Villani theory the displacement interpolation on graphs has been used to introduce a notion of Ricci curvature lower bounds for discrete spaces equipped with Markov kernels [9] that implies a variety of functional inequalities in analogy to the theory of Lott–Sturm–Villani. The discrete transport distance $\mathcal{W}$ has been shown to be consistent with optimal transport on continuous domains. It converges in the sense of Gromov–Hausdorff to the continuous 2-Wasserstein distance for a large class of increasingly finer finite-volume discretizations of the domain [13,14]. A related result for the convergence of the discrete gradient flow to the continuous counterpart is given in [8].

In order to fully exploit the potential of discrete optimal transport in applications, for instance to infer fine analytic and geometric information from curvature bounds for graphs, a precise understanding of optimal paths is needed. Unfortunately, this is currently largely open.

1.1 Contribution

In this article we present an efficient scheme for the numerical approximation of optimal transport paths and the distance $\mathcal{W}$ on discrete sets $\mathcal{X}$ equipped with irreducible Markov kernels Q as introduced by Maas. We use this scheme to exhibit several structural properties of optimal paths in typical examples. For instance, we show that mass is transported not neccesarily only along shortest paths in the underlying graphs, see Sect. 2.1 for more details.

We pick up the Benamou–Brenier-type formulation and provide a temporal discretization of the action functional to obtain a finite-dimensional convex problem and prove Γ-convergence of the discretized functional to the original problem, as well as strong convergence of the discrete geodesics to the continuous geodesics. To overcome the strong coupling of mass variables along graph edges caused by the mass averaging function θ, we introduce a set of slack variables to remedy this entanglement. This allows us to apply a robust proximal point algorithm for the optimization. Due to the slack variables, all involved proximal mappings can be computed efficiently by either solving a sparse linear program (if Q is sparse) or by decomposing them into independent low-dimensional sub-problems.

In particular this numerical scheme does not depend critically on the choice of θ and can be quickly adapted to different variants. We provide formulas for the logarithmic and geometric mean. For a series of numerical test cases we visualize and discuss the behaviour of the interpolating flow. Finally, we adopt the algorithm to approximate gradient flows with respect to the discrete transportation distance $\mathcal{W}$. In particular, we test the algorithm against a classical backward Euler discretization of the heat equation on a graph which coincides with the gradient flow of the entropy.

1.2 Connection to the literature

Computing classical Wasserstein distances W_2 numerically is often a challenge. While the classical Kantorovich formulation via transport couplings is a standard linear program, its naïve dense form requires $(\mathrm{card}\mathcal{X})^2$ variables which may quickly become computationally unfeasible as $\mathcal{X}$ increases in size. On arbitrary metric graphs $(\mathcal{X}, d)$ an additional problem arises: only local edge lengths are usually prescribed and the full distance function $d : \mathcal{X} \times \mathcal{X} \to \mathbb{R}$ is in general unknown a priori. On large graphs, computing d from local edge lengths may be computationally prohibitive or even storing d may exceed the memory capacities.

Owing to its particular structure, the 1-Wasserstein distance over a discrete graph can be reformulated as a min cost flow problem along its edges, thus drastically reducing the number of required variables if the graph is sparse and requiring no precomputation of d, see for instance [2]. On continuous domains this corresponds to *Beckmann's problem* [22]. A numerical scheme tailored to application on meshed surfaces is presented in [23]. A computational approach that uses quadratic regularization to break the non-uniqueness of the optimal flow is described in [12].

For the 2-Wasserstein distance on continuous domains the Benamou–Brenier formula serves a similar purpose, see for instance [21] for a numerical scheme based on

proximal point algorithms. However, this does not immediately carry over to discrete graphs, as the mass averaging function θ introduces a non-trivial coupling of the mass variables along graph edges. In [24] a Benamou–Brenier-type transport distance on discrete metric graphs is developed, similar to the construction of Maas, and a corresponding numerical scheme is developed. A crucial design choice is that θ is picked to be the harmonic mean which allows the application of second-order convex cone programs for numerical optimization. This does not extend to other choices of θ and thus, for instance, hinders the numerical study of the gradient flow when θ is the logarithmic mean.

1.3 Organization

The paper is organized as follows. First we review the construction of the discrete transport metric on graphs by Maas [16] in Sect. 2. Then, in Sect. 3 we will derive the time discretization and establish Γ-convergence of the time discrete action functional and the convergence of time discrete geodesics to a time continuous geodesic. Next, the proximal splitting algorithm with suitably chosen slack variables is presented in detail in Sect. 4. Numerical results are discussed in Sect. 5 and the experimental comparison of solutions of a JKO scheme for the entropy and solutions of the Markov semigroup are presented in Sect. 6.

2 Optimal transport on graphs

In this section we briefly review the discrete transportation metric on the space of probability measures over a graph and in particular recall the basic definitions and discuss the analogy to the L^2-Wasserstein metric on probability measures over $\mathbb{R}^n$. Then we derive a priori bounds on feasible curves of measures.

2.1 The discrete transportation distance

Let $\mathcal{X}$ be a finite set and let $Q : \mathcal{X} \times \mathcal{X} \to [0, \infty)$ be the transition rate matrix of a continuous time Markov chain on $\mathcal{X}$. I.e. we have $Q(x, y) \geq 0$ for $x \neq y$ and make the convention that $Q(x, x) = 0$ for all $x \in \mathcal{X}$. Then $\mathcal{X}$ can be interpreted as the set of vertices of a graph with directed edges (x, y) for those $(x, y) \in \mathcal{X} \times \mathcal{X}$ with positive weight $Q(x, y)$. We assume the Markov chain to be irreducible or equivalently the corresponding graph to be strongly connected. Thus, there exists a unique stationary distribution $\pi : \mathcal{X} \to (0, 1]$ of the Markov chain with $\sum_{x\in\mathcal{X}} \pi(x) = 1$. We further assume that the Markov chain is reversible with respect to π, i.e. the detailed balance condition $\pi(x)Q(x, y) = \pi(y)Q(y, x)$ holds for all $x, y \in \mathcal{X}$. Now, the set of probability densities on $\mathcal{X}$ with respect to π is given by

$$\mathcal{P}(\mathcal{X}) := \left\{ \rho : \mathcal{X} \to \mathbb{R}_0^+ : \sum_{x\in\mathcal{X}} \pi(x)\rho(x) = 1 \right\}.$$

For brevity, in the following we will write $\mathbb{R}^{\mathcal{X}}$ and $\mathbb{R}^{\mathcal{X}\times\mathcal{X}}$ for the spaces of real functions over $\mathcal{X}$ and $\mathcal{X}\times\mathcal{X}$ respectively.

Next, we define the following inner products on $\mathbb{R}^{\mathcal{X}}$ and $\mathbb{R}^{\mathcal{X}\times\mathcal{X}}$

$$\langle \phi, \psi\rangle_\pi := \sum_{x\in\mathcal{X}} \phi(x)\psi(x)\pi(x), \quad \langle \Phi, \Psi\rangle_Q := \frac{1}{2}\sum_{x,y\in\mathcal{X}} \Phi(x,y)\Psi(x,y)Q(x,y)\pi(x) \tag{1}$$

for $\phi, \psi \in \mathbb{R}^{\mathcal{X}}$ and $\Phi, \Psi \in \mathbb{R}^{\mathcal{X}\times\mathcal{X}}$. The corresponding induced norms are denoted by $\|\cdot\|_\pi$ and $\|\cdot\|_Q$. A discrete gradient $\nabla_{\mathcal{X}} : \mathbb{R}^{\mathcal{X}} \to \mathbb{R}^{\mathcal{X}\times\mathcal{X}}$ and a discrete divergence $\mathrm{div}_{\mathcal{X}} : \mathbb{R}^{\mathcal{X}\times\mathcal{X}} \to \mathbb{R}^{\mathcal{X}}$ are given by

$$\begin{aligned}(\nabla_{\mathcal{X}}\psi)(x,y) &:= \psi(x) - \psi(y),\\ (\mathrm{div}_{\mathcal{X}}\Psi)(x) &:= \frac{1}{2}\sum_{y\in\mathcal{X}} Q(x,y)(\Psi(y,x) - \Psi(x,y)).\end{aligned} \tag{2}$$

Then the duality between these two operators formulated as the discrete integration by parts formula

$$\langle \phi, \mathrm{div}_{\mathcal{X}}\Psi\rangle_\pi = -\langle \nabla_{\mathcal{X}}\phi, \Psi\rangle_Q$$

can easily be verified. The associated discrete Laplace-operator $\Delta_{\mathcal{X}} : \mathbb{R}^{\mathcal{X}} \to \mathbb{R}^{\mathcal{X}}$ is given by

$$\Delta_{\mathcal{X}}\psi(x) := \mathrm{div}_{\mathcal{X}}(\nabla_{\mathcal{X}}\psi)(x) = \sum_{y\in\mathcal{X}} Q(x,y)\,[\psi(y) - \psi(x)] = (Q - D)\psi(x)\,,$$

where $D = \mathrm{diag}(\sum_y Q(x,y))_{x\in\mathcal{X}}$. The graph divergence allows to formulate a continuity equation for time-dependent probability densities $\rho : [0,1] \to \mathbb{R}^{\mathcal{X}}$ and momenta $m : [0,1] \to \mathbb{R}^{\mathcal{X}\times\mathcal{X}}$ describing the flow of mass along the graph edges. In explicit, we consider the following definition of solutions to the continuity equation with boundary values at time $t = 0$ and $t = 1$.

Definition 2.1 *(Continuity equation)* The set $\mathcal{CE}(\rho_A, \rho_B)$ of solutions of the continuity equations for given boundary data $\rho_A, \rho_B \in \mathcal{P}(\mathcal{X})$ is defined as the set of all pairs (ρ, m) with $\rho : [0,1]\times\mathbb{R}^{\mathcal{X}} \to \mathbb{R}$ and $m : [0,1]\times\mathbb{R}^{\mathcal{X}\times\mathcal{X}} \to \mathbb{R}$ measurable, such that

$$\begin{aligned}\int_0^1 \langle \partial_t\varphi(t,\cdot), \rho(t,\cdot)\rangle_\pi + \langle \nabla_{\mathcal{X}}\varphi(t,\cdot), m(t,\cdot)\rangle_Q \,\mathrm{d}t\\ = \langle \varphi(1,\cdot), \rho_B\rangle_\pi - \langle \varphi(0,\cdot), \rho_A\rangle_\pi\end{aligned} \tag{3}$$

for all $\varphi \in C^1([0,1], \mathbb{R}^{\mathcal{X}})$.

For $m \in L^2((0,1), \mathbb{R}^{\mathcal{X}\times\mathcal{X}})$ (see Lemma 2.5) one gets $\rho \in H^{1,2}((0,1), \mathbb{R}^{\mathcal{X}})$ and thus $\partial_t \rho + \mathrm{div}_{\mathcal{X}} m = 0$ holds a.e.. Furthermore, $\rho \in C^{0,\frac{1}{2}}([0,1], \mathbb{R}^{\mathcal{X}\times\mathcal{X}})$ and $\rho(1,\cdot) = \rho_B$, $\rho(0,\cdot) = \rho_A$. If $\rho(t,\cdot) \geq 0$ is ensured for all $t \in (0,1)$ via a finite energy property (see (5) below), then testing with $\varphi(t,x) = \zeta(t)$ implies that $\rho(t,\cdot) \in \mathcal{P}(\mathcal{X})$.

The Benamou–Brenier formula [3] asserts that the squared L^2-Wasserstein distance for probability measures in $\mathbb{R}^n$ is the minimum of an action functional over solutions to the corresponding continuity equation. Formally the action functional can be interpreted as a Riemannian path length [20]. To construct an analogous action functional for solutions $(\rho, m) \in \mathcal{CE}(\rho_A, \rho_B)$ a mass density on edges has to be deduced from the the mass densities on the edge nodes. To this end, one defines an averaging function $\theta : (\mathbb{R}_0^+)^2 \to \mathbb{R}_0^+$ which satisfies:

θ is continuous, concave, 1-homogeneous, and symmetric, θ is C^∞ on $(0,+\infty)^2$, $\theta(0,s) = \theta(s,0) = 0$ and $\theta(s,s) = s$ for $s \in \mathbb{R}_0^+$, $\theta(s,t) > 0$ if $s > 0$ and $t > 0$, and $s \mapsto \theta(t,s)$ is monotone increasing on $\mathbb{R}_0^+$ for fixed $t \in \mathbb{R}_0^+$.

It will be useful to consider θ as a concave function $\mathbb{R}^2 \to \mathbb{R} \cup \{-\infty\}$. Therefore, we will set $\theta(s,t) = -\infty$ when $\min\{s,t\} < 0$. Possible choices for θ are for example the logarithmic mean $\theta_{\log}$ or the geometric mean θ_{geo} for $s, t \in \mathbb{R}_0^+$:

$$\theta_{\log}(s,t) = \begin{cases} 0, & \text{if } s = 0 \text{ or } t = 0 \\ s, & \text{if } s = t \\ \frac{t-s}{\log(t)-\log(s)} & \text{otherwise} \end{cases}, \qquad \theta_{\mathrm{geo}}(s,t) = \sqrt{st}. \tag{4}$$

Note that the arithmetic mean is not admissible. Based on this averaging function one can define the discrete transportation distance on $\mathcal{P}(\mathcal{X})$.

Definition 2.2 (Action functional and distance) The action functional for measurable functions $\rho : [0,1] \to \mathbb{R}^{\mathcal{X}}$ and $m : [0,1] \to \mathbb{R}^{\mathcal{X}\times\mathcal{X}}$ is defined as

$$\mathcal{A}(\rho, m) = \frac{1}{2}\int_0^1 \sum_{x,y\in\mathcal{X}} \alpha\big(\rho(t,x), \rho(t,y), m(t,x,y)\big)\, Q(x,y)\, \pi(x)\, \mathrm{d}t$$

$$\text{with } \alpha : \mathbb{R}^3 \to \mathbb{R} \cup \{\infty\}; \quad (s,t,m) \mapsto \begin{cases} \frac{m^2}{\theta(s,t)} & \text{if } \theta(s,t) > 0, \\ 0 & \text{if } \theta(s,t) = 0 \text{ and } m = 0, \\ +\infty & \text{else.} \end{cases} \tag{5}$$

The energy is then given by

$$\mathcal{E}(\rho, m) = \mathcal{A}(\rho, m) + \mathcal{I}_{\mathcal{CE}(\rho_A,\rho_B)}(\rho, m)\,,$$

where $\mathcal{I}_{\mathcal{CE}(\rho_A,\rho_B)}$ is the indicator functional, which is zero for (ρ, m) in $\mathcal{CE}(\rho_A, \rho_B)$ and ∞ otherwise. The induced discrete transportation distance is obtained by

$$\mathcal{W}(\rho_A, \rho_B) = \sqrt{\inf \mathcal{E}(\rho, m)}. \tag{6}$$

Note that α is convex and lower semi-continuous and $\mathcal{CE}(\rho_A, \rho_B)$ is a convex set. Hence, (6) is a convex optimization problem. In is shown in [16, Theorem 3.8] that the mapping $\mathcal{W} : \mathcal{P}(\mathcal{X}) \times \mathcal{P}(\mathcal{X}) \to \mathbb{R}$ defines a metric on $\mathcal{P}(\mathcal{X})$, provided

$$\int_0^1 \frac{1}{\sqrt{\theta(1-r, 1+r)}} \, \mathrm{d}r < \infty.$$

This is the case for the logarithmic mean $\theta_{\log}$ and the geometric mean θ_{geo}. In [9, Theorem 3.2] it is shown that the infimum in (6) is attained by an optimal pair (ρ, m). The curve $(\rho_t)_{t\in[0,1]}$ is a constant speed geodesic for the distance $\mathcal{W}$, i.e. it holds $\mathcal{W}(\rho_t, \rho_s) = |t - s|\mathcal{W}(\rho_A, \rho_B)$ for all $s, t \in [0, 1]$.

To underpin the importance of numerical approximations to the discrete optimal transport distance, we remark that already for a graph with three vertices the exact solution is unknown. Our consistent numerical approximation allows us to exhibit several qualitative and quantitative properties of optimal transport curves.

In particular, we observe that mass is transported not neccesarily only along shortest paths in the underlying graph. For instance, on the complete graph with three vertices a, b, c and the optimal path connecting Dirac masses in a and b moves mass not only along the edge (a, b) but also along via the vertex c (see Fig. 1). This is in sharp contrast to displacement interpolation on continuous domains, where mass travels only along geodesics. On the other hand, we observe that on a rectangular grid with homogeneous transition rates the optimal transport path between two Dirac masses on the same line is concentrated on this line at any time and does not use further edges (see second row in Fig. 6). Based on the intuition gained via these numerical experiments, both phenomena have been established theoretically in [11] (more generally it can be shown that optimal curves stay concentrated on subgraphs satisfying certain conditions, for instance rectangles on rectangular grids).

Furthermore, we observe that the momentum variable does not necessarily have the same sign during the transport, which is another remarkable effect of the discrete optimal transport distance (see Fig. 2).

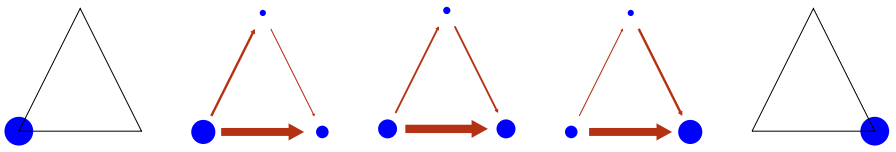

Fig. 1 Optimal transport geodesic on a graph with three nodes. A small amount of mass is transported along the longer way

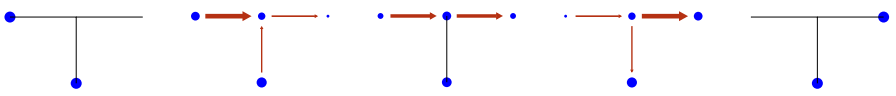

Fig. 2 Optimal transport geodesic on a graph with four nodes. The momentum variable (visualized by red arrows) on the lower edge changes sign during the transport

2.2 A priori bounds

In what follows we will investigate the numerical approximation of $\mathcal{W}$ using a suitable Galerkin discretization in time and solving the resulting discrete convex optimization problem. Here the the nonlinear averaging function θ and the resulting coupling of the values of the probability density on neighbouring nodes will require special treatment in order to obtain a robust and effective solution scheme. To this end, we first discuss a few simplifications of the optimization problem (6) that will help to reduce the computational complexity.

Remark 2.3 (Sparsity of kernel Q) Let $\mathcal{S} = \{(x, y) \in \mathcal{X}^2 : Q(x, y) > 0\}$ be the set of 'edges' indicated by non-zero transition probability. As Q is reversible, one finds $(x, y) \in \mathcal{S}$ iff $(y, x) \in \mathcal{S}$. Furthermore, $\mathrm{div}_{\mathcal{X}} m(t, \cdot)$ and $\mathcal{A}(\rho, m)$ for $m : [0, 1] \to \mathbb{R}^{\mathcal{X}\times\mathcal{X}}$ only depend on values of $m(t, x, y)$ where $(x, y) \in \mathcal{S}$. Hence,if the kernel Q is sparse, i.e. if $\mathcal{S}$ is only a small subset of $\mathcal{X} \times \mathcal{X}$ this implies a considerable reduction of computational complexity.

In addition, the following Lemma allows to replace the two variables $m(t, x, y)$ and $m(t, y, x)$ by one effective variable, further reducing the problem size.

Lemma 2.4 (Antisymmetry of optimal momentum) *If $\mathcal{W}(\rho_A, \rho_B)$ is finite and if $\rho : [0, 1] \to \mathbb{R}^{\mathcal{X}}$ and $m : [0, 1] \to \mathbb{R}^{\mathcal{X}\times\mathcal{X}}$ are optimal for (6) then $m(t, x, y) = -m(t, y, x)$ t-almost everywhere, whenever $(x, y) \in \mathcal{S}$ (see above remark for definition of $\mathcal{S}$).*

Proof Let $\rho : [0, 1] \to \mathbb{R}^{\mathcal{X}}$ and $m : [0, 1] \to \mathbb{R}^{\mathcal{X}\times\mathcal{X}}$ be given such that $\mathcal{E}(\rho, m) < \infty$. Now set

$$\hat{m}(t, x, y) := -m(t, y, x).$$

One quickly verifies that $\mathrm{div}_{\mathcal{X}} \hat{m} = \mathrm{div}_{\mathcal{X}} m$ and that thus $(\rho, \hat{m}) \in \mathcal{CE}(\rho_A, \rho_B)$ as well. Besides, by using that $Q(x, y)\,\pi(x) = Q(y, x)\,\pi(y)$ and $\alpha(s, t, m) = \alpha(t, s, -m)$ one finds that $\mathcal{A}(\rho, \hat{m}) = \mathcal{A}(\rho, m)$. Let now $\overline{m} = \frac{1}{2}(m + \hat{m})$. Note that $\overline{m}(t, x, y)$ is anti-symmetric in x and y. By convexity of $\mathcal{CE}(\rho_A, \rho_B)$ one gets $(\rho, \overline{m}) \in \mathcal{CE}(\rho_A, \rho_B)$ and by convexity of $\mathcal{A}$ one finds

$$\mathcal{A}(\rho, \overline{m}) \le \frac{1}{2}\left(\mathcal{A}(\rho, m) + \mathcal{A}(\rho, \hat{m})\right) = \mathcal{A}(\rho, m).$$

Further, the finiteness of $\mathcal{A}(\rho, m)$ implies that $m(t, x, y) = 0$ when $\theta(\rho(t, x), \rho(t, y)) = 0$ and $(x, y) \in \mathcal{S}$ t-almost everywhere , values of $m(t, x, y)$ for $(x, y) \notin \mathcal{S}$ will have no impact on $\mathcal{A}$, and the function $\mathbb{R} \ni z \mapsto \alpha(s, t, z)$ is even strictly convex for fixed $s, t > 0$. Hence, we observe that $\mathcal{A}(\rho, \overline{m}) < \mathcal{A}(\rho, m)$ unless $\overline{m}$ already coincides with m for almost every t and all $(x, y) \in \mathcal{S}$. □

In the Γ-convergence analysis we will make use on the following L^2 bound for the momentum. Let us introduce the constants

$$C^* := \max_{x\in\mathcal{X}} \sum_y Q(x, y),$$

$$C_* := \min_{x,y\in\mathcal{X}, Q(x,y)>0} Q(x,y)\pi(x). \tag{7}$$

Lemma 2.5 (L^2 bound for the momentum) *Let $(\rho, m) : [0,1] \to \mathbb{R}^{\mathcal{X}} \times \mathbb{R}^{\mathcal{X}\times\mathcal{X}}$ be a measurable path with energy $\mathcal{E}(\rho, m) \le \overline{E} < \infty$. Then, m and ρ are uniformly bounded in $L^2((0,1), \mathbb{R}^{\mathcal{X}\times\mathcal{X}})$ and $H^{1,2}((0,1), \mathbb{R}^{\mathcal{X}}) \cap C^{0,\frac{1}{2}}([0,1], \mathbb{R}^{\mathcal{X}})$, respectively, with bounds solely depending on $\mathcal{X}$ and $\overline{E}$.*

Proof Since $\mathcal{E}(\rho, m) < \infty$, we have $(\rho, m) \in \mathcal{CE}(\rho_A, \rho_B)$, and thus for a.e. $t \in (0,1)$ the mass is preserved, *i.e.* $\sum_{x\in\mathcal{X}} \rho(t,x)\pi(x) = \sum_{x\in\mathcal{X}} \rho_A(x)\pi(x) = 1$. In addition, $\rho(t,x)$ is non-negative for all $x \in \mathcal{X}$ and a.e. $t \in (0,1)$. By symmetry and concavity of θ and since $\theta(s,s) = s$, we can estimate

$$\begin{aligned}\theta(\rho(t,x),\rho(t,y)) &= \frac{1}{2}\theta(\rho(t,x),\rho(t,y)) + \frac{1}{2}\theta(\rho(t,y),\rho(t,x)) \\ &\le \theta\Big(\frac{\rho(t,x)+\rho(t,y)}{2}, \frac{\rho(t,x)+\rho(t,y)}{2}\Big) = \frac{\rho(t,x)+\rho(t,y)}{2}\end{aligned}$$

and get

$$\begin{aligned}&\sum_{x,y\in\mathcal{X}} \theta(\rho(t,x),\rho(t,y))Q(x,y)\pi(x) \le \frac{1}{2}\sum_{x,y\in\mathcal{X}} (\rho(t,x)+\rho(t,y))Q(x,y)\pi(x) \\ &= \sum_{x,y\in\mathcal{X}} \rho(t,x)Q(x,y)\pi(x) \le C^* \sum_{x\in\mathcal{X}} \rho(t,x)\pi(x) = C^*. \end{aligned}\tag{8}$$

Thus, using the Cauchy–Schwarz inequality we obtain

$$\begin{aligned}\Big(\sum_{x,y\in\mathcal{X}} |m(t,x,y)|Q(x,y)\pi(x)\Big)^2 &\le \Big(\sum_{x,y\in\mathcal{X}} \alpha(\rho(t,x),\rho(t,y),m(t,x,y))Q(x,y)\pi(x)\Big) \\ &\quad\cdot \Big(\sum_{x,y\in\mathcal{X}} \theta(\rho(t,x),\rho(t,y))Q(x,y)\pi(x)\Big).\end{aligned}\tag{9}$$

Integrating in time we obtain

$$\int_0^1 ||m(t,\cdot,\cdot)||_Q^2 \,\mathrm{d}t = \int_0^1 \sum_{x,y\in\mathcal{X}} m(t,x,y)^2 Q(x,y)\pi(x)\,\mathrm{d}t \le \frac{C^*}{C_*}\overline{E}.$$

Finally, using the continuity equation (3) and m in $L^2((0,1), \mathbb{R}^{\mathcal{X}\times\mathcal{X}})$ we obtain that

$$\begin{aligned}\int_0^1 ||\partial_t\rho||_\pi^2 \,\mathrm{d}t &\le \int_0^1 \sum_x \Big|\sum_y m(t,x,y)Q(x,y)\Big|^2 \pi(x)dt \\ &\le C^* \int_0^1 \sum_{x,y} m(t,x,y)^2 Q(x,y)\pi(x)dt.\end{aligned}$$

This implies that $\rho \in H^{1,2}((0,1), \mathbb{R}^{\mathcal{X}})$ and via the Sobolev embedding theorem we obtain that also $\rho \in C^{0,\frac{1}{2}}((0,1), \mathbb{R}^{\mathcal{X}})$. □

3 Discretization

3.1 Galerkin discretization

To approximate the minimizers of (6) numerically we choose a Galerkin discretization in time. The time interval $[0,1]$ is divided into N subintervals $I_i = [t_i, t_{i+1})$ for $i = 0, \dots, N-1$ with uniform step size $h = \frac{1}{N}$ and $t_i = i\,h$. Then, we define discrete spaces

$$
\begin{aligned}
V^1_{n,h} &= \{\psi_h \in C^0([0,1], \mathbb{R}^{\mathcal{X}}) : \ \psi_h(\cdot)|_{I_i} \text{ is affine } \forall i = 0, \dots, N-1\}, \\
V^0_{n,h} &= \{\psi_h : [0,1] \to \mathbb{R}^{\mathcal{X}} : \ \psi_h(\cdot)|_{I_i} \text{ is constant } \forall i = 0, \dots, N-1\}, \\
V^0_{e,h} &= \{\psi_h : [0,1] \to \mathbb{R}^{\mathcal{X}\times\mathcal{X}} : \ \psi_h(\cdot)|_{I_i} \text{ is constant } \forall i = 0, \dots, N-1\}.
\end{aligned}
$$

For a function $\psi_h \in V^0_{n,h}$ or $V^0_{e,h}$ we will often write $\psi_h(t_i)$ to refer to its value on the interval $I_i = [t_i, t_{i+1})$. For a function $\psi_h \in V^1_{n,h}$ the time-derivative can be interpreted as map

$$
\partial_t : V^1_{n,h} \to V^0_{n,h}, \quad (\partial_t \psi_h)(t_i) = \frac{1}{h}(\psi_h(t_{i+1}) - \psi_h(t_i)) \text{ for } i = 0, \dots, N-1.
$$

We pick $V^1_{n,h} \times V^0_{e,h}$ as the space for discretized masses and momenta (ρ_h, m_h). That is, discrete masses ρ_h are continuous and piecewise affine and the corresponding momenta m_h will be piecewise constant. $\partial_t \rho_h$ and $\mathrm{div}_{\mathcal{X}} m_h$ then lie in $V^0_{n,h}$. In analogy to Definition 2.1 we define discrete solutions of the continuity equation.

Definition 3.1 The set of solutions to the discretized continuity equation for given boundary values $\rho_A, \rho_B \in \mathbb{R}^{\mathcal{X}}$ is given by

$$
\begin{aligned}
\mathcal{CE}_h(\rho_A, \rho_B) = \Big\{ (\rho_h, m_h) \in V^1_{n,h} \times V^0_{e,h} \ : \ & h \sum_{i=0}^{N-1} \langle \partial_t \rho_h(t_i, \cdot) \\
& + \mathrm{div}_{\mathcal{X}} m_h(t_i, \cdot), \varphi_h(t_i, \cdot) \rangle_\pi = 0 \ \forall \varphi_h \in V^0_{n,h}, \\
& \rho_h(t_0, x) = \rho_A(x), \rho_h(t_N, x) = \rho_B(x) \Big\}. \qquad (10)
\end{aligned}
$$

One can quickly verify that $\mathcal{CE}_h(\rho_A, \rho_B) = \mathcal{CE}(\rho_A, \rho_B) \cap (V^1_{n,h} \times V^0_{e,h})$ and that $\partial_t \rho_h + \mathrm{div}_{\mathcal{X}} m_h = 0$ holds for a.e. t when $(\rho_h, m_h) \in \mathcal{CE}_h(\rho_A, \rho_B)$. Next, we define a fully discrete action functional in analogy to Definition 2.2 and subsequently a discrete version of the transport metric $\mathcal{W}$.

Definition 3.2 *(Time-discrete action and transportation distance)* The averaging operator avg_h takes a measure $\psi \in \mathcal{M}([0,1], \mathbb{R}^{\mathcal{X}})$ to its average values on time intervals I_i:

$$\mathrm{avg}_h : \mathcal{M}([0,1], \mathbb{R}^{\mathcal{X}}) \to V^0_{n,h}, \quad (\mathrm{avg}_h\, \psi)(t_i) = \psi(I_i) \ \text{ for } i = 0, \dots, N-1.$$

Analogously we declare the avg_h operator for $\mathbb{R}^{\mathcal{X}\times\mathcal{X}}$-valued measures. Note that for $\psi_h \in V^1_{n,h}$ one finds $(\mathrm{avg}_h\, \psi_h)(t_i) = \frac{1}{2}(\psi_h(t_i) + \psi_h(t_{i+1}))$. For $(\rho, m) \in \mathcal{M}([0,1], \mathbb{R}^{\mathcal{X}}) \times \mathcal{M}([0,1], \mathbb{R}^{\mathcal{X}\times\mathcal{X}})$ the discrete approximation for the action is given by

$$\begin{aligned}\mathcal{A}_h(\rho, m) &= \mathcal{A}(\mathrm{avg}_h\, \rho, \mathrm{avg}_h\, m) \\ &= \frac{h}{2} \sum_{i=0}^{N-1} \sum_{x,y\in\mathcal{X}} \alpha\left(\mathrm{avg}_h\, \rho(t_i, x), \mathrm{avg}_h\, \rho(t_i, y), \mathrm{avg}_h\, m(t_i, x, y)\right) Q(x, y)\pi(x).\end{aligned}$$

Finally, the time discrete energy functional is defined by $\mathcal{E}_h(\rho, m) = \mathcal{A}_h(\rho, m) + \mathcal{I}_{\mathcal{CE}_h(\rho_A,\rho_B)}(\rho, m)$ and for the associated time discrete approximation of the transportation distance one obtains

$$\mathcal{W}_h(\rho_A, \rho_B) = \sqrt{\inf \mathcal{E}_h(\rho, m)}. \tag{11}$$

Note that the indicator function of the discrete continuity equation entails the constraint $(\rho, m) \in V^1_{n,h} \times V^0_{e,h}$. These spaces can be represented by finite-dimensional vectors, the operators ∂_t and avg_h can be represented as finite-dimensional matrices and the continuity equation becomes a finite-dimensional affine constraint. Thus, (11) is indeed a finite-dimensional convex optimization problem. Its numerical solution by using proximal mappings will be detailed in Sect. 4.

3.2 Γ-convergence

In the following, we will prove a Γ-convergence result of the discrete energy functional, which will justify our discretization. First, we construct explicitly continuous and discrete trajectories between an arbitrary probability distribution on $\mathcal{X}$ and the uniform probability density $\mathbb{I} \in \mathcal{P}(\mathcal{X})$ given by $\mathbb{I}(x) = 1$. We show that these trajectories have uniformly bounded energy, which will be essential in the Γ-lim sup inequality in Theorem 3.6. Let us define the Lagrange interpolation operator $\mathcal{I}_h : C^0([0,1], \mathbb{R}^{\mathcal{X}}) \to V^1_{n,h}$; $\rho \mapsto \mathcal{I}_h(\rho)$ given by

$$(\mathcal{I}_h\, \rho)\,(t_i, x) := \rho(t_i, x) \quad \forall i = 0, \dots, N.$$

Proposition 3.3 *There is some constant $C(\mathcal{X}) < \infty$ such that for any $\rho_A \in \mathcal{P}(\mathcal{X})$ there is a trajectory $(\rho, m) \in \mathcal{CE}(\rho_A, \mathbb{I})$ with $\mathcal{A}(\rho, m) \le C(\mathcal{X})$ and $(\mathcal{I}_h\, \rho, \mathrm{avg}_h\, m) \in \mathcal{CE}_h(\rho_A, \mathbb{I})$ with $\mathcal{A}_h(\mathcal{I}_h\, \rho, \mathrm{avg}_h\, m)) \le C(\mathcal{X})$ for every $h = 1/N$.*

Proof For $x \in \mathcal{X}$ let $\rho_A^x \in \mathcal{P}(\mathcal{X})$ be the probability density on $\mathcal{X}$ with all mass concentrated on x. That is, $\rho_A^x = \frac{1}{\pi(x)}\delta_x$, where δ_x is the usual Kronecker symbol with $\delta_x(y) = 1$ if $x = y$ and 0 else.

Construction of elementary flows For $(x, y) \in \mathcal{X} \times \mathcal{X}$, $x \neq y$, with $Q(x, y) > 0$ we define $L[x, y] \in \mathbb{R}^{\mathcal{X}\times\mathcal{X}}$ as follows:

$$L[x, y](a, b) = \begin{cases} \frac{1}{Q(x,y)\,\pi(x)} & \text{if } (a, b) = (x, y), \\ \frac{-1}{Q(x,y)\,\pi(x)} & \text{if } (a, b) = (y, x), \\ 0 & \text{else.} \end{cases}$$

Then $\mathrm{div}_{\mathcal{X}} L[x, y] = \rho_A^y - \rho_A^x$. Now, for any $(x, y) \in \mathcal{X} \times \mathcal{X}$, $x \neq y$, there exists a path $(x = x_0, x_1, \ldots, x_K = y)$ with $K < \mathrm{card}\,\mathcal{X}$ with $Q(x_k, x_{k+1}) > 0$ for $k = 0, \ldots, K - 1$. We can add the corresponding $L[x_k, x_{k+1}]$ along these edges to construct a flow $M[x, y]$ with $\mathrm{div}_{\mathcal{X}} M[x, y] = \rho_A^y - \rho_A^x$. All entries of all $M[x, y]$ are bounded (in absolute value) by $\widetilde{C}(\mathcal{X}) := \mathrm{card}\mathcal{X}/C_*$, where C_* is defined in (7). For $x = y$, $M[x, x]$ is simply zero.

Now assume $\rho_A = \rho_A^x$ for some $x \in \mathcal{X}$. Let $m_0 = \sum_{y\in\mathcal{X}} M[x, y]\,\pi(y)$. One finds

$$\mathrm{div}_{\mathcal{X}} m_0 = \sum_{y\in\mathcal{X}} \left(\tfrac{1}{\pi(y)}\delta_y - \tfrac{1}{\pi(x)}\delta_x\right)\pi(y) = \mathbb{I} - \rho_A^x.$$

Again, every entry of m_0 is bounded in absolute value by $\widetilde{C}(\mathcal{X})$. Now let $m(t) = 2\,m_0\,t$, $\rho(t) = \rho_A^x + (\mathrm{div}_{\mathcal{X}} m_0)\,t^2 = (1 - t^2)\cdot\rho_A^x + t^2\cdot\mathbb{I}$. We find $(\rho, m) \in \mathcal{CE}(\rho_A^x, \mathbb{I})$. One has $|m(t, x, y)| \leq t \cdot 2\widetilde{C}(\mathcal{X})$ and $\rho(t, x) \geq t^2$ and using the monotonicity of α for the action $\mathcal{A}$ we get

$$\mathcal{A}(\rho, m) \leq \frac{1}{2}\int_0^1 \sum_{x,y\in\mathcal{X}} \frac{(t \cdot 2\widetilde{C}(\mathcal{X}))^2}{t^2} Q(x, y)\,\pi(x)\ \mathrm{d}t = 2\widetilde{C}(\mathcal{X})^2 C^*.$$

Construction of discrete counterparts For fixed $h = 1/N$ let $\rho_h = \mathcal{I}_h\,\rho$ and $m_h = \mathrm{avg}_h\,m$. By construction $(\rho_h, m_h) \in \mathcal{CE}_h(\rho_A^x, \mathbb{I})$. Then, one finds $m_h(t_i, x, y) \leq (i + \frac{1}{2})\,h\,2\widetilde{C}(\mathcal{X})$, $\rho_h(t_i, x) \geq i^2\,h^2$, $(\mathrm{avg}_h\,\rho_h)(t_i, x) \geq (i^2 + i + \frac{1}{2})\,h^2$, and thus

$$\begin{aligned}\mathcal{A}_h(\rho_h, m_h) &= \mathcal{A}(\mathrm{avg}_h\,\rho_h, m_h) \\ &\leq \frac{1}{2}\sum_{i=0}^{N-1} h \frac{h^2\,4\widetilde{C}(\mathcal{X})^2\,(i + \frac{1}{2})^2}{h^2(i^2 + i + \frac{1}{2})} \sum_{x,y\in\mathcal{X}} Q(x, y)\,\pi(x) \leq 2\widetilde{C}(\mathcal{X})^2 C^*.\end{aligned}$$

Extension for arbitrary initial data For given $x \in \mathcal{X}$ let (ρ^x, m^x) be the (continuous) trajectory between ρ_A^x and $\mathbb{I}$ as constructed above. Any ρ_A is a superposition of various ρ_A^x:

$$\rho_A = \sum_{x\in\mathcal{X}} \rho_A(x)\,\delta_x = \sum_{x\in\mathcal{X}} \rho_A(x)\pi(x)\,\rho_A^x$$

By linearity of the continuity equation the trajectory $(\rho, m) = \sum_{x\in\mathcal{X}} \rho_A(x)\,\pi(x)\cdot(\rho^x, m^x)$ then lies in $\mathcal{CE}(\rho_A, \mathbb{I})$. Since $\mathcal{A}$ is convex and 1-homogeneous, it is sub-additive. Therefore,

$$\mathcal{A}(\rho, m) \le \sum_{x\in\mathcal{X}} \rho_A(x)\,\pi(x)\,\mathcal{A}(\rho^x, m^x) \le \sum_{x\in\mathcal{X}} \rho_A(x)\,\pi(x)\,2\,\widetilde{C}(\mathcal{X})^2 C^* = 2\,\widetilde{C}(\mathcal{X})^2 C^*.$$

For the discrete trajectory the reasoning is completely analogous. Thus the claim follows with $C(\mathcal{X}) = 2\,\widetilde{C}(\mathcal{X})^2 C^*$. □

Corollary 3.4 *The above strategy can be used to construct trajectories between arbitrary ρ_A, ρ_B via $\mathbb{I}$ as intermediate state. This establishes that $\mathcal{W}$ and $\mathcal{W}_h$ are uniformly bounded on $\mathcal{P}(\mathcal{X})^2$.*

Remark 3.5 In [16] it is shown that $\mathcal{W}$ is bounded if the constant $C_\theta := \int_0^1 \frac{1}{\sqrt{\theta(1-r,1+r)}}\,\mathrm{d}r$ is finite. Here, we assumed that $\theta(s, s) = s$ for $s \in \mathbb{R}_0^+$ and that $s \mapsto \theta(s, t)$ is increasing on $\mathbb{R}_0^+$ for fixed $t \in \mathbb{R}_0^+$ which implies that $\theta(s, t) \ge \min\{s, t\}$ for $s,\ t \in \mathbb{R}_0^+$. This is sufficient for $C_\theta < \infty$.

Theorem 3.6 (Γ-convergence of time discrete energies) *Let ρ_A, ρ_B be fixed temporal boundary conditions. Then, the sequence of functionals $(\mathcal{E}_h)_h$ Γ-converges for $h \to 0$ to the functional $\mathcal{E}$ with respect to the weak$*$ topology in $\mathcal{M}([0, 1], \mathbb{R}^{\mathcal{X}} \times \mathbb{R}^{\mathcal{X}\times\mathcal{X}})$.*

Proof To establish Γ-convergence, we have to verify the Γ-lim inf and Γ-lim sup properties.

For the Γ-lim inf property, we have to demonstrate that the inequality

$$\mathcal{A}(\rho, m) + \mathcal{I}_{\mathcal{CE}(\rho_A,\rho_B)}(\rho, m) \le \liminf_{h\to 0} \mathcal{A}_h(\rho_h, m_h) + \mathcal{I}_{\mathcal{CE}_h(\rho_A,\rho_B)}(\rho_h, m_h) \quad (12)$$

holds for all sequences $(\rho_h, m_h) \overset{*}{\rightharpoonup} (\rho, m)$ in $\mathcal{M}([0, 1], \mathbb{R}^{\mathcal{X}} \times \mathbb{R}^{\mathcal{X}\times\mathcal{X}})$. As $\mathcal{CE}(\rho_A, \rho_B)$ is weak-$*$ closed and $\mathcal{CE}_h(\rho_A, \rho_B) \subset \mathcal{CE}(\rho_A, \rho_B)$ the statement is trivial if there is no subsequence with $(\rho_h, m_h) \in \mathcal{CE}_h(\rho_A, \rho_B)$. Thus, we may assume that all (ρ_h, m_h) fulfill the discrete continuity equation, that (ρ, m) fulfills the continuous continuity equation, and all ρ_h are non-negative.

Now, $\rho_h \overset{*}{\rightharpoonup} \rho$ implies $\mathrm{avg}_h\,\rho_h \overset{*}{\rightharpoonup} \rho$ and $\mathcal{A}_h(\rho_h, m_h) = \mathcal{A}(\mathrm{avg}_h\,\rho_h, m_h)$. Since α is jointly convex and lower semi-continuous in ρ and m, the action functional $\mathcal{A}$ is weak-$*$ lower semi-continuous and (12) holds.

To verify the Γ-lim sup property we need to show that for any $(\rho, m) \in \mathcal{M}([0,1], \mathbb{R}^{\mathcal{X}} \times \mathbb{R}^{\mathcal{X}\times\mathcal{X}})$ there exists a recovery sequence $(\rho_h, m_h) \overset{*}{\rightharpoonup} (\rho, m)$ with

$$\limsup_{h\to 0} \mathcal{A}_h(\rho_h, m_h) + \mathcal{I}_{\mathcal{CE}_h(\rho_A,\rho_B)}(\rho_h, m_h) \le \mathcal{A}(\rho, m) + \mathcal{I}_{\mathcal{CE}(\rho_A,\rho_B)}(\rho, m). \quad (13)$$

We may assume $\mathcal{A}(\rho, m) < \infty$ and $(\rho, m) \in \mathcal{CE}(\rho_A, \rho_B)$. Using Lemma 2.5 this implies in particular that $\rho \in C^{0,\frac{1}{2}}([0,1], \mathbb{R}^{\mathcal{X}})$. For such a trajectory (ρ, m) we will construct a recovery sequence in two steps: First, the continuous trajectory (ρ, m) is regularized. Then, this regularized trajectory, which is still continuous in time, is discretized using local averaging in time. The regularization is necessary to control the effect of the discontinuity of α at the origin, see (5).

Let $(\rho_{A,\mathbb{I}}, m_{A,\mathbb{I}}) \in \mathcal{CE}(\rho_A, \mathbb{I})$ be the trajectory from ρ_A to $\mathbb{I}$ as constructed in Proposition 3.3, analogously let $(\rho_{\mathbb{I},B}, m_{\mathbb{I},B}) \in \mathcal{CE}(\mathbb{I}, \rho_B)$ be the corresponding trajectory from $\mathbb{I}$ to ρ_B with $(\rho_{\mathbb{I},B}, m_{\mathbb{I},B})(t,\cdot) := (\rho_{B,\mathbb{I}}, -m_{B,\mathbb{I}})(1-t,\cdot)$. Then, for $\delta \in (0, \frac{1}{2})$ and $\epsilon = \delta^2$ we define

$$\rho_\delta(t) = \begin{cases} (1-\epsilon)\cdot\rho_A + \epsilon\cdot\rho_{A,\mathbb{I}}(t/\delta) & \text{for } t \in [0,\delta), \\ (1-\epsilon)\cdot\rho((t-\delta)/(1-2\delta)) + \epsilon\cdot\mathbb{I} & \text{for } t \in [\delta, 1-\delta), \\ (1-\epsilon)\cdot\rho_B + \epsilon\cdot\rho_{\mathbb{I},B}((t-(1-\delta))/\delta) & \text{for } t \in [1-\delta, 1] \end{cases}$$

and

$$m_\delta(t) = \begin{cases} \epsilon\cdot\delta^{-1}\cdot m_{A,\mathbb{I}}(t/\delta) & \text{for } t \in [0,\delta), \\ (1-\epsilon)\cdot(1-2\delta)^{-1}\cdot m((t-\delta)/(1-2\delta)) & \text{for } t \in [\delta, 1-\delta), \\ \epsilon\cdot\delta^{-1}\cdot m_{\mathbb{I},B}((t-(1-\delta))/\delta) & \text{for } t \in [1-\delta, 1]. \end{cases}$$

One finds that $(\rho_\delta, m_\delta) \in \mathcal{CE}(\rho_A, \rho_B)$. To evaluate the action of (ρ_δ, m_δ) we decompose it into the contributions of the time intervals $I_l = [0,\delta]$, $I_m = [\delta, 1-\delta]$ and $I_r = [1-\delta, 1]$:

$$\mathcal{A}(\rho_\delta, m_\delta) = \mathcal{A}_l + \mathcal{A}_m + \mathcal{A}_r \qquad \text{with}$$
$$\mathcal{A}_\chi = \int_{I_\chi} \mathcal{A}^{\text{int}}(\rho_\delta(t), m_\delta(t))\,\mathrm{d}t \text{ for } \chi \in \{l, m, r\}.$$

where

$$\mathcal{A}^{\text{int}} : \mathbb{R}^{\mathcal{X}} \times \mathbb{R}^{\mathcal{X}\times\mathcal{X}} \to \mathbb{R}\cup\{\infty\},$$
$$(\rho, m) \mapsto \frac{1}{2}\sum_{x,y\in\mathcal{X}} \alpha\big(\rho(x), \rho(y), m(x,y)\big)\, Q(x,y)\,\pi(x).$$

$\mathcal{A}^{\mathrm{int}}$ is jointly convex and 1-homogeneous and therefore sub-additive. Moreover, it is 2-homogeneous in the second argument. Therefore we obtain

$$\begin{aligned}\mathcal{A}_m &\le \frac{(1-\epsilon)}{(1-2\delta)^2}\int_{I_m}\mathcal{A}^{\mathrm{int}}\big(\rho((t-\delta)/(1-2\delta)), m((t-\delta)/(1-2\delta))\big)\,\mathrm{d}t\\ &= \frac{(1-\epsilon)}{(1-2\delta)}\int_0^1 \mathcal{A}^{\mathrm{int}}\big(\rho(t), m(t)\big)\,\mathrm{d}t = \frac{(1-\epsilon)}{(1-2\delta)}\mathcal{A}(\rho, m).\end{aligned}$$

Further, using Proposition 3.3 we obtain $\mathcal{A}_l + \mathcal{A}_r \le 2\,C(\mathcal{X})\,\delta$.

Next, we discretize in time. Since $\rho \in C^{0,\frac{1}{2}}([0,1],\mathbb{R}^{\mathcal{X}})$ we have $|\rho(t,x) - \rho(t',x)| \le g(|t-t'|)$ with $g(s) := C\cdot s^{\frac{1}{2}}$ for all $x\in\mathcal{X}$. Now let $\Delta = g(2h)$ and choose the regularization parameter $\delta = \min\{i\cdot h : i\in\mathbb{N},\, i\cdot h \ge \Delta^{\frac{1}{4}}\}$ and as before $\epsilon = \delta^2$. Obviously Δ, δ and $\epsilon\to 0$ as $h\to 0$. In particular, for h sufficiently small $2 \ge 1/(1-2\delta)$ and thus $\Delta = g(2h) \ge g(h/(1-2\delta))$. Therefore, Δ is a uniform upper bound for the variation of ρ_δ on any interval of the size h. We now set

$$\rho_h = \mathcal{I}_h\,\rho_\delta, \quad m_h = \mathrm{avg}_h\, m_\delta\,,$$

and note that $(\rho_h, m_h)\in\mathcal{CE}_h(\rho_A,\rho_B)$. As $\delta\to 0$ one finds $(\rho_\delta, m_\delta)\overset{*}{\rightharpoonup}(\rho,m)$ and for $h\to 0$ we obtain $(\rho_\delta-\rho_h, m_\delta - m_h)\overset{*}{\rightharpoonup} 0$. This implies that $(\rho_h,m_h)\overset{*}{\rightharpoonup}(\rho,m)$.

Note that δ was chosen to be an integer multiple of h. So the division of $[0,1]$ into the three intervals $[0,\delta]$, $[\delta,1-\delta]$ and $[1-\delta,1]$ in the construction of (ρ_δ, m_δ) is compatible with the grid discretization of step size h. Therefore, as above, the discrete action decomposes into three contributions which we denote $\mathcal{A}_h(\rho_h,m_h) = \mathcal{A}_{l,h} + \mathcal{A}_{m,h} + \mathcal{A}_{r,h}$. Again, using joint 1-homogeneity and sub-additivity of α, as well as the 2-homogeneity in the second argument one obtains

$$\mathcal{A}_{l,h} \le \frac{\epsilon}{\delta}\cdot\mathcal{A}_h(\mathcal{I}_h\,\rho_{A,\mathbb{I}}, \mathrm{avg}_h\, m_{A,\mathbb{I}}), \quad \mathcal{A}_{r,h}\le\frac{\epsilon}{\delta}\cdot\mathcal{A}_h(\mathcal{I}_h\,\rho_{\mathbb{I},B}, \mathrm{avg}_h\, m_{\mathbb{I},B}).$$

Using Proposition 3.3 we observe that

$$\mathcal{A}_{l,h} + \mathcal{A}_{r,h} \le 2\,C(\mathcal{X})\,\delta.$$

In view of (14), it remains to estimate $\mathcal{A}_{m,h}$ by a suitable constant times $\mathcal{A}_m$. To this end, let $S_m\subset\{0,\dots,N-1\}$ the the set of discrete indices such that $I_i\subset I_m$ for $i\in S_m$. Then $\mathcal{A}_m$ is given by

$$\mathcal{A}_m = \frac{1}{2}\sum_{i\in S_m}\sum_{x,y\in\mathcal{X}}\left[\int_{I_i}\alpha\big(\rho_\delta(t,x),\rho_\delta(t,y),m_\delta(t,x,y)\big)\,\mathrm{d}t\right]Q(x,y)\,\pi(x).$$

Since α is convex, by Jensen's inequality one finds

$$\int_{I_i}\alpha\big(\rho_\delta(t,x),\rho_\delta(t,y),m(t,x,y)\big)\,\mathrm{d}t \ge h\cdot\alpha$$

$$\big((\mathrm{avg}_h\,\rho_\delta)(t_i,x),(\mathrm{avg}_h\,\rho_\delta)(t_i,y),(\mathrm{avg}_h\,m_\delta)(t_i,x,y)\big).$$

The discretized action $\mathcal{A}_{m,h}$ is a weighted sum of the form

$$\mathcal{A}_{m,h}=\frac{h}{2}\sum_{i\in S_m}\sum_{x,y\in\mathcal{X}}\alpha\\ \big((\mathrm{avg}_h\,\mathcal{I}_h\,\rho_\delta)(t_i,x),(\mathrm{avg}_h\,\mathcal{I}_h\,\rho_\delta)(t_i,y),(\mathrm{avg}_h\,m_\delta)(t_i,x,y)\big)Q(x,y)\,\pi(x)\,.$$

By construction ρ_δ is bounded from below by ϵ on I_m on all nodes and its variation within each discretization interval is bounded by Δ. Therefore, for any $i\in S_m, z\in\mathcal{X}$ one finds

$$(\mathrm{avg}_h\,\rho_\delta)(t_i,z)\le(\mathrm{avg}_h\,\mathcal{I}_h\,\rho_\delta)(t_i,z)+\Delta\,,\quad(\mathrm{avg}_h\,\mathcal{I}_h\,\rho_\delta)(t_i,z)\ge\epsilon.$$

Due to the monotonicity of $s\to\frac{s}{s+\Delta}$ we obtain

$$\frac{(\mathrm{avg}_h\,\mathcal{I}_h\,\rho_\delta)(t_i,z)}{(\mathrm{avg}_h\,\rho_\delta)(t_i,z)}\ge\frac{(\mathrm{avg}_h\,\mathcal{I}_h\,\rho_\delta)(t_i,z)}{(\mathrm{avg}_h\,\mathcal{I}_h\,\rho_\delta)(t_i,z)+\Delta}\ge\frac{\epsilon}{\epsilon+\Delta}.$$

Taking into account the joint 1-homogeneity of θ and the monotonicity of θ in each single argument this implies for all $x,y\in\mathcal{X}$ that

$$\frac{\theta\big((\mathrm{avg}_h\,\mathcal{I}_h\,\rho_\delta)(t_i,x),(\mathrm{avg}_h\,\mathcal{I}_h\,\rho_\delta)(t_i,y)\big)}{\theta\big((\mathrm{avg}_h\,\rho_\delta)(t_i,x),(\mathrm{avg}_h\,\rho_\delta)(t_i,y)\big)}\ge\frac{\epsilon}{\epsilon+\Delta}=\frac{1}{1+\Delta/\epsilon}.$$

Hence,

$$\begin{aligned}\mathcal{A}_{m,h}&=\frac{1}{2}\sum_{i\in S_m}\sum_{x,y\in\mathcal{X}}h\cdot\frac{(\mathrm{avg}_h\,m_\delta)^2(t_i,x,y)}{\theta((\mathrm{avg}_h\,\mathcal{I}_h\,\rho_\delta)(t_i,x),(\mathrm{avg}_h\,\mathcal{I}_h\,\rho_\delta)(t_i,y))}Q(x,y)\,\pi(x)\\&\le\frac{1}{2}(1+\Delta/\epsilon)\sum_{i\in S_m}\sum_{x,y\in\mathcal{X}}h\cdot\frac{(\mathrm{avg}_h\,m_\delta)^2(t_i,x,y)}{\theta((\mathrm{avg}_h\,\rho_\delta)(t_i,x),(\mathrm{avg}_h\,\rho_\delta)(t_i,y))}Q(x,y)\,\pi(x)\\&=(1+\Delta/\epsilon)\mathcal{A}_m.\end{aligned}$$

Our choice of δ implies that $\epsilon=\delta^2\ge\Delta^{\frac{1}{2}}$ and thus $\Delta/\epsilon\le\epsilon$. Altogether, we obtain for h sufficiently small

$$\mathcal{A}_h(\rho_h,m_h)=\mathcal{A}_{l,h}+\mathcal{A}_{m,h}+\mathcal{A}_{r,h}\le 2\,C(\mathcal{X})\,\delta+(1+\epsilon)\,\frac{1-\epsilon}{1-2\delta}\,\mathcal{A}(\rho,m).$$

Since $\delta\to 0,\epsilon\to 0$ as $h\to 0$, this establishes the Γ-lim sup property. □

Next, we establish convergence of the discrete optimizers to a continuous solution. To establish compactness we first show a uniform bound for the L^2 norm of the discrete momenta, in analogy to Lemma 2.5.

Lemma 3.7 (L^2 bound for the discrete momentum) *Let $(\rho_h, m_h) \in V^1_{n,h} \times V^0_{e,h}$ with discrete energy $\mathcal{E}_h(\rho_h, m_h) \leq \overline{E} < \infty$. Then, there exists a constant $\overline{M} < \infty$ only depending on $(\mathcal{X}, Q, \pi)$ and $\overline{E}$ (and not on h), such that $\|m_h\|_{L^2([0,1],\mathbb{R}^{\mathcal{X}\times\mathcal{X}})} \leq \overline{M}$.*

Proof The proof works in complete analogy to Lemma 2.5. We bound

$$\begin{aligned}
&\left(\sum_{x,y\in\mathcal{X}} |m_h(t_i, x, y)|Q(x, y)\pi(x)\right)^2 \\
&\leq \left(\sum_{x,y\in\mathcal{X}} \alpha(\mathrm{avg}_h\, \rho_h(t_i, x), \mathrm{avg}_h\, \rho_h(t_i, y), m_h(t_i, x, y))Q(x, y)\pi(x)\right) \\
&\quad \cdot \left(\sum_{x,y\in\mathcal{X}} \theta(\mathrm{avg}_h\, \rho_h(t_i, x), \mathrm{avg}_h\, \rho_h(t_i, y))Q(x, y)\pi(x)\right)
\end{aligned}$$

and

$$\sum_{x,y\in\mathcal{X}} \theta(\mathrm{avg}_h\, \rho_h(t_i, x), \mathrm{avg}_h\, \rho_h(t_i, y))\, Q(x, y)\pi(x) \leq C^*,$$

where C^* is defined in (7). Here, we have used that $(\rho_h, m_h) \in \mathcal{CE}(\rho_A, \rho_B)$ which implies that mass is preserved, *i.e.* $\sum_{x\in\mathcal{X}} \mathrm{avg}_h\, \rho_h(t_i, x)\pi(x) = \sum_{x\in\mathcal{X}} \rho_h(t_i + \frac{h}{2}, x)\pi(x) = \sum_{x\in\mathcal{X}} \rho_A(x)\pi(x) = 1$ for all $i = 0, \ldots, N-1$, and that since $\mathcal{A}_h(\rho_h, m_h) < \infty$ one has $\mathrm{avg}_h\, \rho_h \geq 0$. Now, once more using that $\mathcal{X}$ is finite and integrating (or summing) in time establishes the bound. □

Theorem 3.8 (Convergence of discrete geodesics) *For fixed temporal boundary conditions ρ_A, ρ_B any sequence (ρ_h, m_h) of minimizers of $\mathcal{E}_h$ is uniformly bounded in $C^{0,\frac{1}{2}}([0, 1], \mathbb{R}^{\mathcal{X}}) \times L^2((0, 1), \mathbb{R}^{\mathcal{X}\times\mathcal{X}})$ for $h \to 0$. Up to selection of a subsequence, $\rho_h \to \rho$ strongly in $C^{0,\alpha}([0, 1], \mathbb{R}^{\mathcal{X}})$ for any $\alpha \in [0, \frac{1}{2})$ and $m_h \to m$ weakly in L^2 with (ρ, m) being a minimizer of the energy $\mathcal{E}$.*

Proof For a sequence of minimizers (ρ_h, m_h) the discrete energy $\mathcal{E}_h(\rho_h, m_h)$ is uniformly bounded by Corollary 3.4 . Since $(\rho_h, m_h) \in \mathcal{CE}(\rho_A, \rho_B)$ the total variation of all ρ_h is uniformly bounded. Further, by Lemma 3.7 the L^2 norm $\|m_h\|_{L^2([0,1],\mathbb{R}^{\mathcal{X}\times\mathcal{X}})}$ is uniformly bounded. Hence, the sequence $(\rho_h, m_h)_h$ has a weakly$*$ (in the sense of measures) convergent subsequence, which by Theorem 3.6 and a standard consequence of Γ convergence theory converges weakly$*$ to some minimizer (ρ, m) of $\mathcal{E}$).

Using the continuity equation this convergence can be strengthened. We already know that (ρ_h, m_h) solves the continuity equation $\partial_t \rho_h = -\mathrm{div}_{\mathcal{X}} m_h$. Thus, the uniform bound for m_h in $L^2((0, 1), \mathbb{R}^{\mathcal{X}\times\mathcal{X}})$ implies that ρ_h is uniformly bounded in $H^{1,2}(\mathbb{R}^{\mathcal{X}})$. From this we obtain by the Sobolev embedding theorem that $(\rho_h)_h$ is uniformly bounded in $C^{0,\frac{1}{2}}(\mathbb{R}^{\mathcal{X}})$ and compact in $C^{0,\alpha}(\mathbb{R}^{\mathcal{X}})$ for all $\alpha \in [0, \frac{1}{2})$. □

4 Optimization with proximal splitting

4.1 Slack variables and proximal splitting

The computation of the discrete transportation distance (11) and the associated transport path require the solution of a finite-dimensional non-smooth convex optimization problem. To this end, we apply a proximal splitting approach with suitably chosen slack variables. The proximal mapping of a convex and lower semi-continuous function $f : H \to \mathbb{R} \cup \{\infty\}$ on a Hilbert space H with norm $\|\cdot\|_H$ is defined as

$$\operatorname{prox}_f(x) = \operatorname*{arg\,min}_{y \in H} \frac{1}{2}\|x - y\|_H^2 + f(y). \tag{14}$$

Furthermore, the indicator function of a closed convex set $K \subset H$ is given by $\mathcal{I}_K(x) = 0$ for $x \in K$ and ∞ elsewise. In particular, $\operatorname{prox}_{\mathcal{I}_K} = \operatorname{proj}_K$, where proj_K is the projection onto K. For a function $f : H \mapsto \mathbb{R} \cup \{\infty\}$ its Fenchel conjugate is given by

$$f^*(y) = \sup_{x \in H} \langle y, x \rangle_H - f(x). \tag{15}$$

If $f(x) < \infty$ for some $x \in H$, then f^* is convex and lower semi-continuous. For more details and an introduction to convex analysis see e.g. [4]. The practical applicability of proximal splitting schemes depends on whether the objective can be split into terms such that the proximal mapping for each term can be computed efficiently. In [21] a spatiotemporal discretization with staggered grids of the classical Benamou–Brenier formulation [3] of optimal transport of Lebesgue densities on $\mathbb{R}^n$ was presented and several proximal splitting methods were considered to solve the discrete problem. However, this approach can not directly be transfered to problem (11) since the action $\mathcal{A}$ couples the variables ρ and m in a non-linear way via the terms $\alpha(\operatorname{avg}_h \rho(t_i, x), \operatorname{avg}_h \rho(t_i, y), m(t_i, x, y))$ spatially over the whole graph according to the transition kernel Q and temporally via the averaging operator avg_h. Thus, the proximal mapping of the $\mathcal{A}$-term is not separable in space or time and thus requires the solution of a fully coupled, nonlinear minimization problem. As a remedy, we propose to introduce auxiliary variables to decouple the variables and rewrite the action $\mathcal{A}$ with terms where variables only interact locally, thus leading to separable, hence simpler, proximal mappings.

Lemma 4.1 *For $(\rho, m) \in V_{n,h}^1 \times V_{e,h}^0$ one finds*

$$\mathcal{A}_h(\rho, m) = \mathcal{A}(\operatorname{avg}_h \rho, m) = \inf \left\{ \widehat{\mathcal{A}}(\vartheta, m) + \mathcal{I}_{\mathcal{K}_{pre}}(\operatorname{avg}_h \rho, \vartheta) \colon \vartheta \in V_{e,h}^0 \right\} \tag{16}$$

with the convex set

$$\mathcal{K}_{pre} := \Big\{ (\bar{\rho}, \vartheta) \in V_{n,h}^0 \times V_{e,h}^0 \colon 0 \le \vartheta(t_i, x, y)$$

$$\leq \theta(\bar\rho(t_i,x),\bar\rho(t_i,y))\,\forall i=0,\dots,N-1,\ \forall x,y\in\mathcal{X}\} \tag{17}$$

and the edge-based action

$$\widehat{\mathcal{A}}(\vartheta,m) := \frac{1}{2}\int_0^1 \sum_{x,y\in\mathcal{X}} \Phi(\vartheta(t,x,y),m(t,x,y))\,Q(x,y)\,\pi(x)\,\mathrm{d}t$$

$$\text{with}\quad \Phi(\vartheta,m) := \begin{cases} \frac{m^2}{\vartheta} & \text{if } \vartheta>0,\\ 0 & \text{if } (m,\vartheta)=(0,0),\\ +\infty & \text{else.}\end{cases} \tag{18}$$

Note that Φ is the integrand of the Benamou–Brenier action functional and that $\alpha(s,t,m)=\Phi(\theta(s,t),m)$.

Proof The first equality is merely the definition of $\mathcal{A}_h$ and using the fact that $\mathrm{avg}_h\, m = m$ for $m\in V^0_{e,h}$. For the second equality note that for any $\vartheta\in V^0_{e,h}$ with $(\bar\rho,\vartheta)\in\mathcal{K}_{\mathrm{pre}}$ one has $\vartheta(t_i,x,y)\leq\theta(\bar\rho(t_i,x),\bar\rho(t_i,y))$. By monotonicity of Φ in its first argument this implies $\Phi(\vartheta(t_i,x,y),m(t_i,x,y))\geq\alpha(\bar\rho(t_i,x),\bar\rho(t_i,y),m(t_i,x,y))$ and hence

$$\mathcal{A}(\bar\rho,m)\leq\inf\left\{\widehat{\mathcal{A}}(\vartheta,m)+\mathcal{I}_{\mathcal{K}_{\mathrm{pre}}}(\bar\rho,\vartheta):\vartheta\in\mathbb{R}^{\mathcal{X}\times\mathcal{X}}\right\}. \tag{19}$$

Further, we obviously have that $\bar\vartheta(t_i,x,y):=\theta(\bar\rho(t_i,x),\bar\rho(t_i,y))$ satisfies $(\bar\rho,\vartheta)\in\mathcal{K}_{\mathrm{pre}}$ and $\widehat{\mathcal{A}}(\bar\vartheta,m)=\mathcal{A}(\bar\rho,m)$. Hence, we have equality in (19). □

The proximal mapping of the function $\widehat{\mathcal{A}}$ can be computed separately for each time interval and graph edge. However, the set $\mathcal{K}_{\mathrm{pre}}$ still couples the variables $\mathrm{avg}_h\,\rho$ and ϑ according to the graph structure and the averaging operator avg_h couples the variables of ρ in time. To resolve this, we introduce a second set of auxiliary variables. We refer already here to the diagram in Fig. 3, which sketches the use of these auxiliary variables in the proximal splitting scheme.

Lemma 4.2 *For $\bar\rho\in V^1_{n,h}$, $\vartheta\in V^0_{e,h}$ one finds*

$$\mathcal{I}_{\mathcal{K}_{pre}}(\mathrm{avg}_h\,\rho,\vartheta)=\inf\Big\{\mathcal{I}_{\mathcal{J}_{avg}}(\rho,\bar\rho)+\mathcal{I}_{\mathcal{J}_=}(\bar\rho,q)+\mathcal{I}_{\mathcal{J}_\pm}(q,\rho^-,\rho^+)$$
$$+\mathcal{I}_{\mathcal{K}}(\rho^-,\rho^+,\vartheta):(\bar\rho,q,\rho^-,\rho^+)\in(V^0_{n,h})^2\times(V^0_{e,h})^2\Big\} \tag{20}$$

where

$$\mathcal{J}_{avg} := \left\{(\rho,\bar\rho)\in V^1_{n,h}\times V^0_{n,h}:\ \bar\rho=\mathrm{avg}_h\,\rho\right\}, \tag{21}$$

$$\mathcal{J}_= := \left\{(\bar\rho,q)\in(V^0_{n,h})^2:\ \bar\rho=q\right\}, \tag{22}$$

$$\mathcal{J}_\pm := \Big\{(q,\rho^-,\rho^+)\in V^0_{n,h}\times(V^0_{e,h})^2 : q(t_i,x) = \rho^-(t_i,x,y),\ q(t_i,y)=\rho^+(t_i,x,y)\Big\}, \tag{23}$$

$$\mathcal{K} := \left\{ (\rho^-, \rho^+, \vartheta) \in (V^0_{e,h})^3 \,:\, (\rho^-(t_i, x, y), \rho^+(t_i, x, y), \vartheta(t_i, x, y)) \in K \right\}, \tag{24}$$

with

$$K := \{(\rho^-, \rho^+, \vartheta) \in \mathbb{R}^3 \,:\, 0 \le \vartheta \le \theta(\rho^-, \rho^+)\}. \tag{25}$$

Proof For fixed $\rho \in V^1_{n,h}$ there is precisely one tuple $(\bar\rho, q, \rho^-, \rho^+)$ such that

$$(\rho, \bar\rho) \in \mathcal{J}_{avg}, \quad (\bar\rho, q) \in \mathcal{J}_{=}, \text{ and } \quad (q, \rho^-, \rho^+) \in \mathcal{J}_{\pm},$$

given by $\bar\rho = \mathrm{avg}_h\, \rho$, $q = \bar\rho$, $\rho^-(t_i, x, y) = q(t_i, x)$, $\rho^+(t_i, x, y) = q(t_i, y)$. For this (ρ^-, ρ^+) one finds $(\rho^-, \rho^+, \vartheta) \in \mathcal{K}$ if and only if $(\mathrm{avg}_h\, \rho, \vartheta) \in \mathcal{K}_{\mathrm{pre}}$. □

The function $\mathcal{I}_{\mathcal{J}_{avg}}$ relates the values of ρ on time nodes to the average values on the adjacent time intervals, $\mathcal{I}_{\mathcal{J}_\pm}$ communicates the values of q on graph nodes to the adjacent graph edges and $\mathcal{I}_{\mathcal{K}}$ ensures the mass averaging via the function θ. The additional splitting via $\mathcal{I}_{\mathcal{J}_=}$ will later simplify partition of the final optimization problem into primal and dual component. The sets $\mathcal{J}_{avg}$, $\mathcal{J}_=$, $\mathcal{J}_\pm$ and $\mathcal{K}$ are all products of simpler low-dimensional sets, implying simpler computation of the relevant proximal mappings and projections.

This gives us an equivalent formulation for the discrete minimization problem (11):

$$\begin{aligned} \mathcal{W}_h(\bar\rho_A, \bar\rho_B)^2 = \inf \Big\{ &(\mathcal{F} + \mathcal{G})(\rho_h, m_h, \vartheta_h, \rho_h^-, \rho_h^+, \bar\rho_h, q_h) \,: \\ &(\rho_h, m_h, \vartheta_h, \rho_h^-, \rho_h^+, \bar\rho_h, q_h) \in V^1_{n,h} \times (V^0_{e,h})^4 \times (V^0_{n,h})^2 \Big\} \end{aligned} \tag{26}$$

with

$$\begin{aligned} \mathcal{F}(\rho_h, m_h, \vartheta_h, \rho_h^-, \rho_h^+, \bar\rho_h, q_h) &:= \widehat{\mathcal{A}}(\vartheta_h, m_h) + \mathcal{I}_{\mathcal{J}_\pm}(q_h, \rho_h^-, \rho_h^+) + \mathcal{I}_{\mathcal{J}_{avg}}(\rho_h, \bar\rho_h), \\ \mathcal{G}(\rho_h, m_h, \vartheta_h, \rho_h^-, \rho_h^+, \bar\rho_h, q_h) &:= \mathcal{I}_{\mathcal{CE}_h(\rho_A, \rho_B)}(\rho_h, m_h) \\ &\quad + \mathcal{I}_{\mathcal{K}}(\rho_h^-, \rho_h^+, \vartheta_h) + \mathcal{I}_{\mathcal{J}_=}(\bar\rho_h, q_h). \end{aligned}$$

The structure of this optimization problem is well suited for the first order primal-dual algorithm presented in [7]. We consider the Hilbert space $H = V^1_{n,h} \times (V^0_{e,h})^4 \times (V^0_{n,h})^2$ composed of tuples of functions in space and time with the scalar product

$$\begin{aligned} &\langle \left(\rho_{h,1}, m_{h,1}, \vartheta_{h,1}, \rho^-_{h,1}, \rho^+_{h,1}, \bar\rho_{h,1}, q_{h,1}\right), \left(\rho_{h,2}, m_{h,2}, \vartheta_{h,2}, \rho^-_{h,2}, \rho^+_{h,2}, \bar\rho_{h,2}, q_{h,2}\right) \rangle_H \\ &\quad := h \sum_{i=0}^{N} \langle \rho_{h,1}(t_i, \cdot), \rho_{h,2}(t_i, \cdot) \rangle_\pi + h \sum_{i=0}^{N-1} \langle \bar\rho_{h,1}(t_i, \cdot), \bar\rho_{h,2}(t_i, \cdot) \rangle_\pi \\ &\qquad + \langle q_{h,1}(t_i, \cdot), q_{h,2}(t_i, \cdot) \rangle_\pi \end{aligned}$$

$$+ h \sum_{i=0}^{N-1} \langle m_{h,1}(t_i, \cdot), m_{h,2}(t_i, \cdot) \rangle_Q + \langle \vartheta_{h,1}(t_i, \cdot), \vartheta_{h,2}(t_i, \cdot) \rangle_Q$$
$$+ h \sum_{i=0}^{N-1} \langle \rho_{h,1}^-(t_i, \cdot), \rho_{h,2}^-(t_i, \cdot) \rangle_Q + \langle \rho_{h,1}^+(t_i, \cdot), \rho_{h,2}^+(t_i, \cdot) \rangle_Q. \tag{27}$$

and the induced norm denoted by $\|\cdot\|_H$. Then applying [7, Algorithm 1] to solve problem (26) with $\mathcal{F}$, $\mathcal{G} : H \to \mathbb{R} \cup \{\infty\}$ amounts to iteratively compute for initial data $(a^{(0)}, b^{(0)}) \in H^2$ and $\overline{a}^{(0)} = a^{(0)}$

$$\begin{aligned} b^{(\ell+1)} &= \operatorname{prox}_{\sigma \mathcal{F}^*}(b^{(\ell)} + \sigma\, \overline{a}^{(\ell)}), \\ a^{(\ell+1)} &= \operatorname{prox}_{\tau \mathcal{G}}(a^{(\ell)} - \tau\, b^{(\ell+1)}), \\ \overline{a}^{(\ell+1)} &= a^{(\ell+1)} + \lambda \cdot (a^{(\ell+1)} - a^{(\ell)}). \end{aligned} \tag{28}$$

where $\tau, \sigma > 0, \lambda \in [0, 1]$. As demonstrated in [7] the iterates converge to a minimizer in (26) if $\tau \cdot \sigma < 1$. For some $(\rho_h, m_h, \vartheta_h, \rho_h^-, \rho_h^+, \bar{\rho}_h, q_h) \in H$ one finds

$$\mathcal{F}^*(\rho_h, m_h, \vartheta_h, \rho_h^-, \rho_h^+, \bar{\rho}_h, q_h) = \widehat{\mathcal{A}}^*(\vartheta_h, m_h) + \mathcal{I}^*_{\mathcal{J}_\pm}(q_h, \rho_h^-, \rho_h^+) + \mathcal{I}^*_{\mathcal{J}_{avg}}(\rho_h, \bar{\rho}_h)$$

and the proximal mapping $(\rho_h^{\mathrm{pr}}, m_h^{\mathrm{pr}}, \vartheta_h^{\mathrm{pr}}, \rho_h^{-\mathrm{pr}}, \rho_h^{+\mathrm{pr}}, \bar{\rho}_h^{\mathrm{pr}}, q_h^{\mathrm{pr}}) = \operatorname{prox}_{\sigma \mathcal{F}^*}(\rho_h, m_h, \vartheta_h, \rho_h^-, \rho_h^+, \bar{\rho}_h, q_h)$ decomposes as follows:

$$\begin{aligned} (\vartheta_h^{\mathrm{pr}}, m_h^{\mathrm{pr}}) &= \operatorname{prox}_{\sigma \widehat{\mathcal{A}}^*}(\vartheta_h, m_h)\,, \\ (q_h^{\mathrm{pr}}, \rho_h^{-\mathrm{pr}}, \rho_h^{-\mathrm{pr}}) &= \operatorname{prox}_{\sigma \mathcal{I}^*_{\mathcal{J}_\pm}}(q_h, \rho_h^-, \rho_h^+)\,, \\ (\rho_h^{\mathrm{pr}}, \bar{\rho}_h^{\mathrm{pr}}) &= \operatorname{prox}_{\sigma \mathcal{I}^*_{\mathcal{J}_{avg}}}(\rho_h, \bar{\rho}_h). \end{aligned}$$

Likewise, for $(\rho_h^{\mathrm{pr}}, m_h^{\mathrm{pr}}, \vartheta_h^{\mathrm{pr}}, \rho_h^{-\mathrm{pr}}, \rho_h^{+\mathrm{pr}}, \bar{\rho}_h^{\mathrm{pr}}, q_h^{\mathrm{pr}}) = \operatorname{prox}_{\tau \mathcal{G}}(\rho_h, m_h, \vartheta_h, \rho_h^-, \rho_h^+, \bar{\rho}_h, q_h)$ one finds

$$\begin{aligned} (\rho_h^{\mathrm{pr}}, m_h^{\mathrm{pr}}) &= \operatorname{proj}_{\mathcal{CE}_h(\rho_A, \rho_B)}(\rho_h, m_h)\,, \\ (\rho^{-\mathrm{pr}}_h, \rho^{+\mathrm{pr}}_h, \vartheta_h^{\mathrm{pr}}) &= \operatorname{proj}_{\mathcal{K}}(\rho_h^-, \rho_h^+, \vartheta_h)\,, \\ (\bar{\rho}_h^{\mathrm{pr}}, q_h^{\mathrm{pr}}) &= \operatorname{proj}_{\mathcal{J}_=}(\bar{\rho}_h, q_h). \end{aligned}$$

Each of the proximal maps is performed with respect to the norm $\|\cdot\|_H$ restricted to the relevant variables.

In what follows, we will study these maps in detail. As in the proximal splitting algorithm for the classical optimal transport problem proposed in [21] our solution scheme also requires to solve a linear system corresponding to an elliptic equation in space and time and to project pointwise onto the same convex set given as the dual of the classical action functional. Furthermore, the projection onto the set $\mathcal{K}$ encodes the additional nonlinearity given by the averaging operator θ. All auxiliary variables and operators are chosen, such that

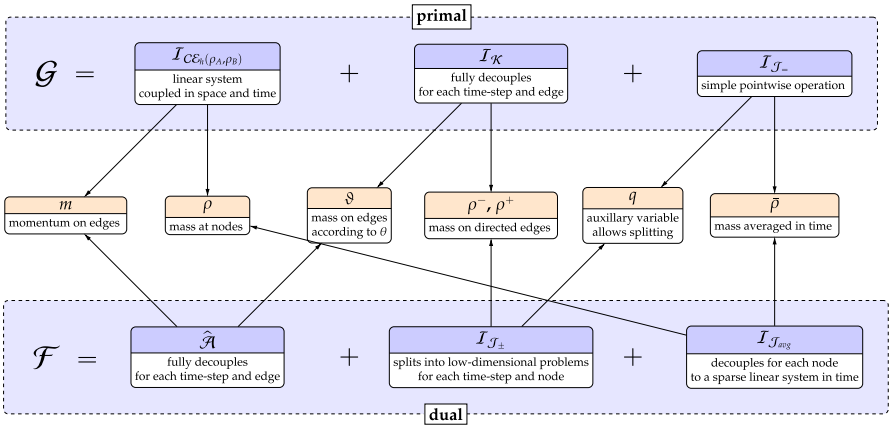

Fig. 3 Sketch of proximal splitting algorithm

- the projection on the three dimensional set K can be performed independently for each time step and each edge,
- the coupling in the original action functional of variables on nodes and variables on edges is effectively decoupled by their distribution among $\mathcal{F}$ and $\mathcal{G}$,
- each variable of $\mathcal{F}$ appears only in one of the component functionals, which allows to decompose the evaluation of $\text{prox}_{\mathcal{F}^*}$.

Consequently, $\text{prox}_{\mathcal{F}^*}$ and $\text{prox}_{\mathcal{G}}$ can be computed efficiently, which ensures that the above scheme is well-suited to solve (26). In Fig. 3 we schematically summarize the splitting underlying our numerical algorithm which in particular highlights the above observations. In what follows we investigate the different proximal mappings used in the algorithm.

4.2 Projection onto $\mathcal{CE}_h(\rho_A, \rho_B)$

For given $(\rho_h, m_h) \in V^1_{n,h} \times V^0_{e,h}$ we need to solve the following problem:

$$\begin{aligned}\text{proj}_{\mathcal{CE}_h(\rho_A,\rho_B)}(\rho_h, m_h) = \underset{(\rho_h^{\text{pr}}, m_h^{\text{pr}}) \in \mathcal{CE}_h(\rho_A,\rho_B)}{\arg\min} \; & \frac{h}{2} \sum_{i=0}^{N} \|\rho_h^{\text{pr}}(t_i,\cdot) - \rho_h(t_i,\cdot)\|_\pi^2 \\ & + \frac{h}{2} \sum_{i=0}^{N-1} \|m_h^{\text{pr}}(t_i,\cdot) - m_h(t_i,\cdot)\|_Q^2 \end{aligned} \tag{29}$$

To this end we take into account the following dual formulation.

Proposition 4.3 *The solution* (ρ_h^{pr}, m_h^{pr}) *to* (29) *is given by*

$$\rho_h^{pr}(t_i,x) = \rho_h(t_i,x) + \frac{\varphi_h(t_i,x) - \varphi_h(t_{i-1},x)}{h}, \quad \forall i = 1,\dots,N-1, \tag{30a}$$

$$\rho_h^{pr}(t_0,x)=\rho_A(x)\,,\ \rho_h^{pr}(t_N,x)=\rho_B(x)\,, \tag{30b}$$

$$m_h^{pr}(t_i,x,y)=m_h(t_i,x,y)+\nabla_{\mathcal{X}}\varphi_h(t_i,x,y)\,,\quad \forall i=0,\dots,N-1. \tag{30c}$$

where φ_h solves the space time elliptic equation

$$\begin{aligned}
&\pi(x)\frac{\varphi_h(t_1,x)-\varphi_h(t_0,x)}{h^2}+\pi(x)\,\triangle_{\mathcal{X}}\varphi_h(t_0,x)\\
&\quad=-\pi(x)\left(\frac{\rho_h(t_1,x)-\rho_A(x)}{h}+\mathrm{div}m_h(t_0,x)\right),\\
&\pi(x)\frac{-\varphi_h(t_{N-1},x)+\varphi_h(t_{N-2},x)}{h^2}+\pi(x)\triangle_{\mathcal{X}}\varphi_h(t_{N-1},x)\\
&\quad=-\pi(x)\left(\frac{\rho_B(x)-\rho_h(t_{N-1},x)}{h}+\mathrm{div}m_h(t_{N-1},x)\right)\\
&\pi(x)\frac{\varphi_h(t_{i+1},x)-2\varphi_h(t_i,x)+\varphi_h(t_{i-1},x)}{h^2}+\pi(x)\,\triangle_{\mathcal{X}}\varphi_h(t_i,x)\\
&\quad=-\pi(x)\left(\frac{\rho_h(t_{i+1},x)-\rho_h(t_i,x)}{h}+\mathrm{div}m_h(t_i,x)\right)
\end{aligned} \tag{31}$$

for $i=1,\dots,N-2$ and $x\in\mathcal{X}$.

The factors $\pi(x)$ in (31) could be canceled but they will simplify further analysis.

Proof We define the Lagrangian corresponding to (29) as

$$\begin{aligned}
L[\rho_h^{\mathrm{pr}},m_h^{\mathrm{pr}},\varphi_h,\lambda_A,\lambda_B]&=\frac{h}{2}\sum_{i=0}^{N}\|\rho_h^{\mathrm{pr}}(t_i,\cdot)-\rho_h(t_i,\cdot)\|_\pi^2\\
&+\frac{h}{2}\sum_{i=0}^{N-1}\|m_h^{\mathrm{pr}}(t_i,\cdot)-m_h(t_i,\cdot)\|_Q^2\\
&+h\sum_{i=0}^{N-1}\sum_{x\in\mathcal{X}}\varphi_h(t_i,x)\left(\frac{\rho_h^{\mathrm{pr}}(t_{i+1},x)-\rho_h^{\mathrm{pr}}(t_i,x)}{h}+\mathrm{div}_{\mathcal{X}}m_h^{\mathrm{pr}}(t_i,x)\right)\pi(x)\\
&+\sum_{x\in\mathcal{X}}\left(\lambda_B(x)(\rho_h^{\mathrm{pr}}(t_N,x)-\rho_B(x))+\lambda_A(x)(\rho_h^{\mathrm{pr}}(t_0,x)-\rho_A(x))\right)\pi(x)
\end{aligned}$$

where λ_A,λ_B are the Lagrange multipliers for the boundary conditions $\rho_h^{\mathrm{pr}}(t_0,\cdot)=\rho_A$, $\rho_h^{\mathrm{pr}}(t_N,\cdot)=\rho_B$. The optimality condition in ρ_h^{pr} and m_h^{pr} directly imply (30a) and (30c). (30b) reflects the boundary conditions, which are to be ensured in $\mathcal{CE}_h(\rho_A,\rho_B)$. Inserting these relations into the continuity equation $\partial_t\rho_h^{\mathrm{pr}}+\mathrm{div}m_h^{\mathrm{pr}}=0$ leads to the system of equations (31). □

The Lagrange multiplier φ_h in Proposition 4.3 lives in $V_{n,h}^0$ which can be identified with $\mathbb{R}^{N\mathrm{card}\mathcal{X}}$. We equip this space with the canonical basis

$$(\varphi_h^{i,x})_{i=0,\dots,N-1,\,x\in\mathcal{X}}\quad\text{where}\quad(\varphi_h^{i,x})(t_j,y)=\delta_{i,j}\cdot\delta_{x,y}$$

and the standard Euclidean inner product with respect to this basis. Then the elliptic equation (31) can be written as a linear system $SZ = F$ for a coordinate vector $Z = (\varphi_h(t_i, x))_{i=0,\dots N-1,\, x\in X}$, a matrix $S \in \mathbb{R}^{(N\mathrm{card}\mathcal{X})\times(N\mathrm{card}\mathcal{X})}$ and a vector $F \in \mathbb{R}^{N\mathrm{card}\mathcal{X}}$. The matrix S is symmetric since $\pi(x)Q(x,y) = \pi(y)Q(y,x)$ and the matrix representation of $\triangle_{\mathcal{X}}$ is $Q - \mathrm{diag}(\sum_y Q(\cdot, y))$. Furthermore, S is sparse if Q is sparse. However, the matrix S is not invertible, its kernel is spanned by functions that are constant in space and time. To see this, assume that a non constant Z is in the kernel of S and denote by ϕ_h the associated function in $V^0_{n,h}$. Now, let $I_+(\mu) := \{(i,x) \in \{0,\dots,N-1\}\times\mathcal{X} : \phi_h(i,x) > \mu\}$ for $\mu = \min \phi_h(i,x)$ and define $\psi_h \in V^0_{n,h}$ via $\psi(t_i,x) = 1$ if $(i,x) \in I_+(\mu)$ and $\psi_h(t_i,x) = 0$ else. Let W be the associated nodal vector to ψ_h. By assumption on Z the set $I_+(\mu)$ is non empty and thus it is easy to see that $W^\top SZ < 0$ and thus Z can not be in the kernel of S, which proves the claim.

We impose the additional constraint $\sum_{i=0}^{N-1}\sum_{x\in\mathcal{X}} \varphi_h(t_i,x) = 0$ to remove this ambiguity. This can be written as $w^\top\varphi_h = 0$ where $w \in \mathbb{R}^{N\mathrm{card}\mathcal{X}}$ is the vector with entries $w^{i,x} = 1$ leading to the linear system

$$\begin{pmatrix} S & w \\ w^T & 0 \end{pmatrix}\begin{pmatrix} Z \\ \lambda \end{pmatrix} = \begin{pmatrix} F \\ 0 \end{pmatrix}.$$

This system is uniquely solvable and the solution implies $\lambda = 0$ if $F \perp w$ (in the Euclidean sense), which is true because ρ_A and ρ_B are assumed to be of equal mass.

4.3 Proximal Mapping of $\widehat{\mathcal{A}}^*$

The function $\widehat{\mathcal{A}}$ is convex and 1-homogeneous, hence its Fenchel conjugate is the indicator function of a convex set and the proximal mapping of $\widehat{\mathcal{A}}^*$ is a projection. For $(\vartheta, m) \in (V^0_{e,h})^2$ one has

$$\widehat{\mathcal{A}}(\vartheta, m) = h\sum_{i=0}^{N-1}\sum_{x,y\in\mathcal{X}} \Phi(\vartheta(t_i,x,y), m(t_i,x,y))\, Q(x,y)\,\pi(x).$$

Following [3] a direct calculation for $(p,q) \in (V^0_{e,h})^2$ yields

$$\begin{aligned}\widehat{\mathcal{A}}^*(p,q) &= \sup_{(\vartheta,m)\in(V^0_{e,h})^2} \frac{h}{2}\sum_{i=0}^{N-1}\Big[\langle p(t_i,\cdot,\cdot), \vartheta(t_i,\cdot,\cdot)\rangle_Q + \langle q(t_i,\cdot,\cdot), m(t_i,\cdot,\cdot)\rangle_Q \\ &\qquad - \frac{1}{2}\sum_{(x,y)\in\mathcal{X}\times\mathcal{X}} \Phi(\vartheta(t_i,x,y), m(t_i,x,y))\, Q(x,y)\,\pi(x)\Big] \\ &= \frac{h}{2}\sum_{\substack{i=0,\dots,N-1\\(x,y)\in\mathcal{X}\times\mathcal{X}}} \Phi^*(p(t_i,x,y), q(t_i,x,y))\, Q(x,y)\,\pi(x)\end{aligned}$$

$$= \sum_{\substack{i=0,\dots,N-1\\(x,y)\in\mathcal{X}\times\mathcal{X}}} \mathcal{I}_{\mathcal{B}}(p(t_i,x,y),q(t_i,x,y))$$

with $\Phi^* = \mathcal{I}_{\mathcal{B}}$ for $\mathcal{B} = \{(p,q) \in \mathbb{R}^2 : p + \frac{q^2}{4} \le 0\}$. Thus the proximal mapping separates into two-dimensional problems for each time interval and graph edge and $(p^{\mathrm{pr}}, q^{\mathrm{pr}}) = \mathrm{prox}_{\sigma\widehat{\mathcal{A}}^*}(p,q)$ precisely if

$$(p^{\mathrm{pr}}(t_i,x,y), q^{\mathrm{pr}}(t_i,x,y)) = \mathrm{proj}_{\mathcal{B}}(p(t_i,x,y),q(t_i,x,y)),$$

where $\mathrm{proj}_{\mathcal{B}}$ is the projection with respect to the standard Euclidean distance on $\mathbb{R}^2$ and a Newton scheme in $\mathbb{R}$ can be used to solve for this projection. Since this proximal mapping is a projection, it is in particular independent of the step size σ.

4.4 Projection onto $\mathcal{K}$

For given $(\rho^-, \rho^+, \vartheta) \in (V^0_{e,h})^3$ we need to solve

$$\begin{aligned}\mathrm{proj}_{\mathcal{K}}(\rho^-,\rho^+,\vartheta) = &\operatorname*{arg\,min}_{(\rho^{-\mathrm{pr}},\rho^{+\mathrm{pr}},\vartheta^{\mathrm{pr}})\in\mathcal{K}} \frac{h}{2}\sum_{i=0}^{N-1}\\ &\Big(\|\rho^{-\mathrm{pr}}(t_i,\cdot,\cdot)-\rho^-(t_i,\cdot,\cdot)\|_Q^2 + \|\rho^{+\mathrm{pr}}(t_i,\cdot,\cdot)-\rho^+(t_i,\cdot,\cdot)\|_Q^2\\ &+ \|\vartheta^{\mathrm{pr}}(t_i,\cdot,\cdot)-\vartheta(t_i,\cdot,\cdot)\|_Q^2\Big).\end{aligned}$$

Recall that $\mathcal{K}$ is a product of the three-dimensional closed convex set K, as indicated in (24). Therefore $(\rho^{-\mathrm{pr}}, \rho^{+\mathrm{pr}}, \vartheta^{\mathrm{pr}}) = \mathrm{proj}_{\mathcal{K}}(\rho^-,\rho^+,\vartheta)$ decouples into the edgewise projection in each time step, i.e.

$$\begin{aligned}&(\rho^{-\mathrm{pr}}(t_i,x,y), \rho^{+\mathrm{pr}}(t_i,x,y), \vartheta^{\mathrm{pr}}(t_i,x,y))\\ &\quad= \mathrm{proj}_K(\rho^-(t_i,x,y),\rho^+(t_i,x,y),\vartheta(t_i,x,y))\end{aligned}$$

where this projection is with respect to the standard Euclidean distance on $\mathbb{R}^3$. Let us denote by $\partial^+\theta(x)$ the super-differential of θ at $x \in \mathbb{R}^2$, which is the analogue of the sub-differential for concave functions. More precisely, $\partial^+\theta(x) = -\partial(-\theta)(x)$, where $\partial(-\theta)(x)$ is the sub-differential of the convex function $x \mapsto -\theta(x)$ at x. Then the projection $p^{\mathrm{pr}} = \mathrm{proj}_K(p)$ of $p \in \mathbb{R}^3$ is characterized by [4, Prop. 6.46]

$$p - p^{\mathrm{pr}} \in N_K(p^{\mathrm{pr}}) := \{z \in \mathbb{R}^3 : \langle z, q - p^{\mathrm{pr}}\rangle \le 0 \,\forall\, q \in K\}, \tag{32}$$

where $N_K(p^{\mathrm{pr}})$ is the normal cone of K at p^{pr}. To solve this inclusion we distinguish the following cases:

Lemma 4.4 *For an averaging function $\theta : \mathbb{R}^2 \to \mathbb{R}$ fulfilling the assumptions listed in Sect. 1 and for $K := \{p \in \mathbb{R}^3 : 0 \le p_3 \le \theta(p_1,p_2)\}$ the normal cone $N_K(p^{pr})$ for $p^{pr} \in K$ is given by:*

(i) *Trivial projection:* $p = p^{pr} \in \operatorname{int} K = \{(p_1, p_2, p_3) \in \mathbb{R}^3 : 0 < p_3 < \theta(p_1, p_2)\}$*, then* $N_K(p^{pr}) = \{0\}$.

(ii) *Projection onto 'bottom facet' of* K*:* $p^{pr} \in (0, +\infty) \times (0, +\infty) \times \{0\}$*, then* $N_K(p^{pr}) = \{0\} \times \{0\} \times \mathbb{R}_0^-$.

(iii) *Projection onto coordinate axis:* $p^{pr} = (p_1^{pr}, 0, 0)$ *for* $p_1^{pr} \in (0, +\infty)$*, then*

$$N_K(p^{pr}) = \{0\} \times \mathbb{R}_0^- \times \mathbb{R}_0^- \cup \left\{(0, q_2, q_3) \in \{0\} \times \mathbb{R}_0^- \times (0, +\infty) : (0, -q_2/q_3) \in \partial^+\theta(p_1^{pr}, 0)\right\}.$$

Note that $(0, q) \in \partial^+\theta(p_1^{pr}, 0)$ *is equivalent to* $q \geq \lim_{z \searrow 0} \partial_2\theta(p_1^{pr}, z)$ *and that* $\partial^+\theta(p_1^{pr}, 0)$ *is empty if* $\lim_{z \searrow 0} \partial_2\theta(p_1^{pr}, z) = \infty$*. The analogous representation holds for the second axis.*

(iv) *Projection onto origin:* $p^{pr} = (0, 0, 0)$*, then*

$$N_K(p^{pr}) = (\mathbb{R}_0^-)^3 \cup \{(q_1, q_2, q_3) \in \mathbb{R}_0^- \times \mathbb{R}_0^- \times (0, +\infty) : (q_1/q_3, q_2/q_3) \in -\partial^+\theta(0)\}.$$

(v) *Projection onto 'upper surface' of* K*:* $p^{pr} = (p_1^{pr}, p_2^{pr}, \theta(p_1^{pr}, p_2^{pr}))$ *for* $(p_1^{pr}, p_2^{pr}) \in (0, +\infty)^2$*, then*

$$N_K(p^{pr}) = \{\lambda \cdot (-\partial_1\theta(p_1^{pr}, p_2^{pr}), -\partial_2\theta(p_1^{pr}, p_2^{pr}), 1) : \lambda \in \mathbb{R}^+\}.$$

Proof For $p^{\mathrm{pr}} \in \operatorname{int} K$ one finds $N_K(p^{\mathrm{pr}}) = \{0\}$ and thus $p^{\mathrm{pr}} = p$, which implies (i).

In case (ii) the set $\mathbb{R} \times \mathbb{R} \times \{0\}$ is obviously the only supporting plane of K that contains p^{pr}. Thus the normal cone is just the ray in direction $(0, 0, -1)$.

Assume $p^{\mathrm{pr}} = (p_1^{\mathrm{pr}}, 0, 0)$, $p_1^{\mathrm{pr}} > 0$. Then there is some $\varepsilon > 0$ such that $\{(p_1^{\mathrm{pr}} + \varepsilon, 0, 0), (p_1^{\mathrm{pr}} - \varepsilon, 0, 0), (p_1^{\mathrm{pr}}, \varepsilon, 0)\} \subset K$. Therefore $N_K(p^{\mathrm{pr}}) \subset \{0\} \times \mathbb{R}_0^- \times \mathbb{R}$. Since $\mathbb{R} \times \{0\} \times \mathbb{R}$ and $\mathbb{R} \times \mathbb{R} \times \{0\}$ are supporting planes of K that contain p^{pr}, one must have $\{0\} \times \mathbb{R}_0^- \times \mathbb{R}_0^- \subset N_K(p^{\mathrm{pr}})$. Moreover, for $\lim_{z \searrow 0} \partial_2\theta(p_1^{\mathrm{pr}}, z) < \infty$ let $z = (z_1, z_2) \in \partial^+\theta(p_1^{\mathrm{pr}}, 0)$. One must have $z_1 = 0$ and $z_2 \in \partial^+ f(0)$ with auxiliary function $f : t \mapsto \theta(p_1^{\mathrm{pr}}, t)$. Then $\{q \in \mathbb{R}^3 : \langle q - p^{\mathrm{pr}}, (0, -z_2, 1)\rangle = 0\}$ is a supporting plane of K and consequently $(0, -z_2, 1) \in N_K(p^{\mathrm{pr}})$. Conversely, from $z_2 \notin \partial^+ f(0)$ follows $(0, -z_2, 1) \notin N_K(p^{\mathrm{pr}})$. So

$$N_K(p^{\mathrm{pr}}) = \{0\} \times \mathbb{R}_0^- \times \mathbb{R}_0^- \cup \{(0, -\lambda \cdot z, \lambda) : z \in \partial^+ f(0), \lambda \in (0, +\infty)\}.$$

The auxiliary function f is concave and by monotonicity of the super-differential we find $\partial^+ f(0) = [\lim_{z \searrow 0} \partial_2\theta(p_1^{\mathrm{pr}}, z), +\infty)$. With this characterization we arrive at the expression for $N_K(p^{\mathrm{pr}})$ as given in (iii). The proof for the second axis is analogous.

For $p^{\mathrm{pr}} = (0, 0, 0)$ we find $(\mathbb{R}_0^-)^3 \subset N_K(0) \subset \mathbb{R}_0^- \times \mathbb{R}_0^- \times \mathbb{R}$ with arguments analogous to those in case (iii). For every $z = (z_1, z_2) \in \partial^+\theta(0)$ a supporting plane through 0 is given by $\{q \in \mathbb{R}^3 : \langle q, (-z_1, -z_2, 1)\rangle = 0\}$ and hence $(-z_1, -z_2, 1) \in N_K(0)$. Conversely, $z = (z_1, z_2) \notin \partial^+\theta(0)$ implies $(-z_1, -z_2, 1) \notin N_K(0)$. With this, one obtains the expression for $N_K(0)$ given in (iv).

Finally, we consider $p^{\mathrm{pr}} = (p_1^{\mathrm{pr}}, p_2^{\mathrm{pr}}, \theta(p_1^{\mathrm{pr}}, p_2^{\mathrm{pr}}))$ with $(p_1^{\mathrm{pr}}, p_2^{\mathrm{pr}}) \in (0, +\infty)^2$. In a neighbourhood of p^{pr}, K is the subgraph of a concave, differentiable function. The unique supporting plane of K through p^{pr} is given by $\{q \in \mathbb{R}^3 : \langle q - p^{\mathrm{pr}}, (-\partial_1\theta(p_1^{\mathrm{pr}}, p_2^{\mathrm{pr}}), -\partial_2\theta(p_1^{\mathrm{pr}}, p_2^{\mathrm{pr}}), 1)\rangle = 0\}$ and $(-\partial_1\theta(p_1^{\mathrm{pr}}, p_2^{\mathrm{pr}}), -\partial_2\theta(p_1^{\mathrm{pr}}, p_2^{\mathrm{pr}}), 1)$ is the unique associated outer normal as stated in (v). □

Using Lemma 4.4 one can devise an algorithm for the projection onto K. For $p = (p_1, p_2, p_3) \in \mathbb{R}^3$ the projection $p^{\mathrm{pr}} = \mathrm{proj}_K(p)$ can be determined as follows:

function PROJECT$K(p_1,p_2,p_3)$
  if $0 \le p_3 \le \theta(p_1, p_2)$ **return** (p_1, p_2, p_3)
  if $p_3 \le 0$ **return** $(\max\{p_1, 0\}, \max\{p_2, 0\}, 0)$
  if $(p_1 > 0) \wedge (p_2 \le 0)$ **then**
    if $-p_2/p_3 \ge \lim_{z \searrow 0} \partial_2\theta(p_1, z)$ **return** $(p_1, 0, 0)$
  end if
  if $(p_1 \le 0) \wedge (p_2 > 0)$ **then**
    if $-p_1/p_3 \ge \lim_{z \searrow 0} \partial_1\theta(z, p_2)$ **return** $(0, p_2, 0)$
  end if
  if $(p_1 \le 0) \wedge (p_2 \le 0)$ **then**
    if $(-p_1/p_3, -p_2/p_3) \in \partial^+\theta(0)$ **return** $(0, 0, 0)$
  end if
  return PROJECTKTOP(p_1,p_2,p_3)
end function

The function PROJECTKTOP(p_1,p_2,p_3) in the above algorithm corresponds to case (v) of Lemma 4.4, where p^{pr} lies on the 'upper surface' of K, defined by the graph surface of θ. It will be described in more detail below. In the following we will occasionally use the curve $c : (0, \infty) \to \mathbb{R}^2;\ q \mapsto (q^{-1/2}, q^{1/2})$ to parametrize orientations in $(0, \infty)^2$. Due to the 1-homogeneity of θ, often it suffices to look at its values at $\theta(c(q))$. Alternative choices for c are feasable as well.

Lemma 4.5 (Projection onto 'upper surface' of K) *Let $p \in \mathbb{R}^3$ with projection on K given by $p^{pr} = (p_1^{pr}, p_2^{pr}, \theta(p_1^{pr}, p_2^{pr}))$ with $(p_1^{pr}, p_2^{pr}) \in (0, +\infty)^2$. Further, let $w(q) = (q^{1/2}, q^{-1/2}, \theta(q^{1/2}, q^{-1/2}))$ be a parametrized curve on the 'upper surface' and $n(q) = (-\partial_1\theta(q^{1/2}, q^{-1/2}), -\partial_2\theta(q^{1/2}, q^{-1/2}), 1)$ be the corresponding normal. Then there exists a unique $(q, \tau) \in (0, \infty)^2$ s.t. $p^{pr} = \tau w(q)$. We have that q is the unique root of $q \mapsto \langle p, w(q) \times n(q)\rangle$ and $\tau = \langle p, \frac{w(q)}{\|w(q)\|^2}\rangle$.*

Proof Since θ is 1-homogeneous, any p^{pr} of the form $(p_1^{\mathrm{pr}}, p_2^{\mathrm{pr}}, \theta(p_1^{\mathrm{pr}}, p_2^{\mathrm{pr}}))$, $(p_1^{\mathrm{pr}}, p_2^{\mathrm{pr}}) \in (0, +\infty)^2$, can be written as $p^{\mathrm{pr}} = \tau \cdot w(q)$ for unique $q \in (0, +\infty)$ and $\tau \in (0, +\infty)$. In explicit, $q = p_1^{\mathrm{pr}}/p_2^{\mathrm{pr}}$ and $\tau = (p_1^{\mathrm{pr}} \cdot p_2^{\mathrm{pr}})^{\frac{1}{2}}$. Now, $n(q)$ is orthogonal on the graph of θ and outward pointing. Hence, p lies in the plane spanned by $w(q)$ and $n(q)$. This is equivalent to $\langle p, w(q) \times n(q)\rangle = 0$. Since p^{pr} is unique, this must be the unique root of $q \mapsto \langle p, w(q) \times n(q)\rangle$. Once q is determined, we know the ray on which p^{pr} lies. To find τ, one must solve the remaining one-dimensional projection onto the ray. Consequently, τ is the unique minimizer of $\tau \mapsto \frac{1}{2}\|p - \tau \cdot w(q)\|^2$, which concludes the proof. □

For case (iv) of Lemma 4.4 we need to characterize the super-differential of θ at the origin.

Lemma 4.6 *The super-differential of θ at the origin is given by*

$$\partial^+\theta(0) = \overline{\{\nabla\theta(q^{-1/2}, q^{1/2}) \,:\, q \in (0,\infty)\}} + (\mathbb{R}_0^+)^2.$$

Proof Due to the 1-homogeneity of θ

$$\begin{aligned}\langle \nabla\theta(\lambda p), \lambda r\rangle &= \lim_{\epsilon\to 0} \frac{\theta(\lambda(p+\epsilon r)) - \theta(\lambda p)}{\epsilon} \\ &= \lambda \lim_{\epsilon\to 0} \frac{\theta(p+\epsilon r) - \theta(p)}{\epsilon} = \lambda\langle \nabla\theta(p), r\rangle\end{aligned}$$

for $p \in (0,+\infty)^2$, $\lambda > 0$, and all $r \in \mathbb{R}^2$, which leads to $\nabla\theta(\lambda p) = \nabla\theta(p)$ for $p \in (0,+\infty)^2$ and $\lambda > 0$. Thus, for the curve $c : (0,\infty) \to \mathbb{R}^2;\ q \mapsto (q^{-1/2}, q^{1/2})$ the set of tangent planes at $(c(q), \theta(c(q)))$ spanned by $(\nabla\theta(c(q)), 1)$ and $(c(s), \theta(c(q)))$ for $q \in (0,\infty)$ is already the complete set of affine tangent planes to the graph of θ over $(0,\infty)^2$. Thus, by continuity of θ on $[0,\infty)^2$ we get $\theta(0) + \langle r, p\rangle \geq \theta(p)$ for $r \in \{\nabla\theta(c(q)) \,:\, q \in (0,\infty)\}$. From this we deduce that $\partial^+\theta(0) \supset \{\nabla\theta(c(q)) \,:\, q \in (0,\infty)\} + (\mathbb{R}_0^+)^2$. Since $\partial^+\theta(0)$ is a closed set [4, Prop. 16.3], this implies

$$\partial^+\theta(0) \supset \overline{\{\nabla\theta(c(s)) \,:\, q \in (0,\infty)\}} + (\mathbb{R}_0^+)^2.$$

Furthermore, for any $w \in \mathbb{R}^2 \setminus \{0\}$ with $w_1,\ w_2 \leq 0$ there exists a p' with $\theta(0) + \langle (r+w), p\rangle < \theta(p')$ Since $\theta(z) = 0$ for $z \in (\{0\} \times \mathbb{R}_0^+) \cup (\mathbb{R}_0^+ \times \{0\})$ and $\theta(z) = -\infty$ outside $[0,\infty)^2$ we finally obtain that $\theta(0) + \langle r, p\rangle \geq \theta(p)$ if and only if $r \in \overline{\{\nabla\theta(c(q)) \,:\, q \in (0,\infty)\}} + (\mathbb{R}_0^+)^2$, which proves the claim. □

Logarithmic mean Now, we turn to the specific case when $\theta = \theta_{\log}$ is the logarithmic mean (4). For $s > 0$ $\lim_{t\searrow 0} \partial_1\theta(t,s) = \lim_{t\searrow 0} \partial_2\theta(s,t) = +\infty$. That is, $N_K(s,0,0) = \{0\} \times \mathbb{R}_0^- \times \mathbb{R}_0^-$ and analogous $N_K(0,s,0) = \mathbb{R}_0^- \times \{0\} \times \mathbb{R}_0^-$. Consequently, the algorithm simplifies as follows:

function PROJECT$K(p_1,p_2,p_3)$
  if $0 \leq p_3 \leq \theta(p_1, p_2)$ **return** (p_1, p_2, p_3)
  if $p_3 \leq 0$ **return** $(\max\{p_1, 0\}, \max\{p_2, 0\}, 0)$
  if $(p_1 \leq 0) \wedge (p_2 \leq 0) \wedge (-p_1/p_3, -p_2/p_3) \in \partial^+\theta(0)$ **return** $(0,0,0)$
  return PROJECTKTOP(p_1,p_2,p_3)
end function

The inclusion in $\partial^+\theta(0)$ can be tested as follows.

Lemma 4.7 *Let $z = (z_1, z_2) \in \mathbb{R}^2$. If $\min\{z_1, z_2\} \leq 0$ then $z \notin \partial^+\theta(0)$. Otherwise, there is a unique $q_1 \in (0,+\infty)$ such that $\partial_1\theta(q_1^{-1/2}, q_1^{1/2}) = z_1$ and then $z \in \partial^+\theta(0)$ if and only if $z_2 \geq \partial_2\theta(q^{-1/2}, q^{1/2})$.*

Proof Note that for the logarithmic mean $\partial^+\theta(0) \subset (0,+\infty)^2$ and therefore $z \notin \partial^+\theta(0)$ if $\min\{z_1, z_2) \leq 0$. One finds that

$$\partial_1\theta(q^{-1/2}, q^{1/2}) = \frac{q-1-\log(q)}{\log^2(q)}$$

is monotone increasing with $\partial_1\theta(q^{-1/2}, q^{1/2}) \to 0$ as $q \to 0$ and $\partial_1\theta(q^{-1/2}, q^{1/2}) \to +\infty$ as $q \to +\infty$. Indeed, for $\beta(q) = \partial_1\theta(q^{-1/2}, q^{1/2})$ with $\beta(1) := \frac{1}{2}$ we obtain a continuous extension on $(0, \infty)$. Furthermore, we consider $\beta'(q) = \frac{2(1-q)+\log(q)(1+q)}{q\log^3(q)}$ with continuous extension $\frac{1}{6}$ for $q = 1$ and verify that $2(1-q)+\log(q)(1+q)$ is negative for $q < 1$ and positive for $q > 1$. This implies that $\beta'(q) > 0$. Furthermore, by symmetry we obtain that $\partial_2\theta(q^{-1/2}, q^{1/2})$ is monotone decreasing with $\partial_2\theta(q^{-1/2}, q^{1/2}) \to +\infty$ as $q \to 0$ and $\partial_2\theta(q^{-1/2}, q^{1/2}) \to 0$ as $q \to +\infty$. By Lemma 4.6

$$\partial^+\theta(0) = \{\nabla\theta(q^{-1/2}, q^{1/2}) : q \in (0,+\infty)\} + (\mathbb{R}_+)^2.$$

Thus, for every $z \in (0,+\infty)^2$ there is a unique $q_1 \in (0,+\infty)$ such that $\partial_1\theta(q_1^{-1/2}, q_1^{1/2}) = z_1$ and $z_1 \geq \partial_1\theta(q^{-1/2}, q^{1/2})$ if and only if $q \leq q_1$. Furthermore, there is a unique $q_2 \in (0,+\infty)$ such that $\partial_2\theta(q_2^{-1/2}, q_2^{1/2}) = z_2$ and $z_2 \geq \partial_2\theta(q^{-1/2}, q^{1/2})$ if and only if $q \geq q_2$. Hence, $z \in \partial^+\theta(0)$ if and only if $q_2 \leq q_1$, which is equivalent to $z_2 \geq \partial_2\theta(q_1^{-1/2}, q_1^{1/2})$. □

Remark 4.8 (Comments on Numerical Implementation) The sought-after q in Lemma 4.7 can be determined with a one-dimensional Newton iteration. The function $q \mapsto \partial_1\theta(q^{-1/2}, q^{1/2})$ becomes increasingly steep as $q \to 0$ which leads to increasingly unstable Newton iterations as z_1 approaches 0. On $q \in [1,+\infty)$ the function is rather flat and easy to invert numerically. To avoid these numerical problems, note that the roles of z_1 and z_2 in Lemma 4.7 can easily be swapped which corresponds to the transformation $q \leftrightarrow q^{-1}$. Moreover, for $\max\{z_1, z_2\} < \frac{1}{2}$ one has $z \notin \partial^+\theta(0)$. With this rule and by swapping the values of z_1 and z_2 if $z_1 < z_2$ one can always remain in the regime $q \in [1,+\infty)$. Additionally, we recommend to replace the function $\theta(s,t)$ and its derivatives by a local Taylor expansion near the numerically unstable diagonal $s = t$.

Geometric mean Furthermore, let us consider the case where $\theta = \theta_{\text{geo}}$ is the geometric mean (4). For $s > 0$ we again find $\lim_{t\searrow 0}\partial_1\theta(t,s) = \lim_{t\searrow 0}\partial_2\theta(s,t) = +\infty$ and consequently the same simplification of the algorithm applies as in the case of the logarithmic mean. For the test of the inclusion $z = (z_1, z_2) \in \partial^+\theta(0)$, we argue as in the proof of Lemma 4.7. The functions $\partial_1\theta(q^{-1/2}, q^{1/2}) = \frac{1}{2}q^{\frac{1}{2}}$ and $\partial_2\theta(q^{-1/2}, q^{1/2}) = \frac{1}{2}q^{-\frac{1}{2}}$ have the same monotonicity properties as for the logarithmic mean. Therefore, if $\min\{z_1, z_2\} \leq 0$ then $z \notin \partial^+\theta(0)$. Otherwise, $q_1 = 4z_1^2$ and thus the condition $\partial_2\theta(q_1^{-1/2}, q_1^{1/2}) \leq z_2$ is equivalent to $z_1 \cdot z_2 \geq \frac{1}{4}$. To summarize, we have obtained

$$\partial^+\theta(0) = \left\{ z \in \mathbb{R}^2 : \, z_1 \cdot z_2 \geq \tfrac{1}{4} \wedge \min\{z_1, z_2\} > 0 \right\}.$$

4.5 Proximal Mapping of $\mathcal{I}^*_{\mathcal{J}_\pm}$

Note that $\mathcal{I}_{\mathcal{J}_\pm}$ is a 1-homogeneous function. Hence, $\mathcal{I}^*_{\mathcal{J}_\pm}$ will once again be an indicator function and $\mathrm{prox}_{\mathcal{I}^*_{\mathcal{J}_\pm}}$ a projection. Consequently, the proximal mapping is independent of the step size σ, i.e. $\mathrm{prox}_{\sigma\,\mathcal{I}^*_{\mathcal{J}_\pm}} = \mathrm{prox}_{\mathcal{I}^*_{\mathcal{J}_\pm}}$. To compute $\mathrm{prox}_{\mathcal{I}^*_{\mathcal{J}_\pm}}$ we use Moreau's decomposition [4, Thm. 14.3] that implies

$$\mathrm{prox}_{\mathcal{I}^*_{\mathcal{J}_\pm}} = \mathrm{id} - \mathrm{prox}_{\mathcal{I}_{\mathcal{J}_\pm}} = \mathrm{id} - \mathrm{proj}_{\mathcal{J}_\pm} \tag{33}$$

where id is the identity map on $V^0_{n,h} \times (V^0_{e,h})^2$. To compute $\mathrm{proj}_{\mathcal{J}_\pm}(\rho, \rho^-, \rho^+)$ for a point $(\rho, \rho^-, \rho^+) \in V^0_{n,h} \times (V^0_{e,h})^2$ one has to find the minimizer $(\rho^{\mathrm{pr}}, \rho^{-\mathrm{pr}}, \rho^{+\mathrm{pr}}) \in \mathcal{J}_\pm$ of

$$\begin{aligned}\sum_{i=0}^{N-1} &\|\rho^{\mathrm{pr}}(t_i, \cdot) - \rho(t_i, \cdot)\|^2_\pi + \|\rho^{-\mathrm{pr}}(t_i, \cdot, \cdot) - \rho^-(t_i, \cdot, \cdot)\|^2_Q \\ &+ \|\rho^{+\mathrm{pr}}(t_i, \cdot, \cdot) - \rho^+(t_i, \cdot, \cdot)\|^2_Q.\end{aligned}$$

Recall that for any $\rho^{\mathrm{pr}} \in V^0_{n,h}$ there is precisely one pair $(\rho^{-\mathrm{pr}}, \rho^{+\mathrm{pr}}) \in (V^0_{e,h})^2$ such that $(\rho^{\mathrm{pr}}, \rho^{-\mathrm{pr}}, \rho^{+\mathrm{pr}}) \in \mathcal{J}_\pm$, see (23). Therefore, one has to find $\rho^{\mathrm{pr}} \in V^0_{n,h}$ which minimizes

$$\begin{aligned}\sum_{i=0}^{N-1} &\sum_{x \in \mathcal{X}} |\rho^{\mathrm{pr}}(t_i, x) - \rho(t_i, x)|^2 \pi(x) \\ &+ \frac{1}{2} \sum_{(x,y) \in \mathcal{X}^2} |\rho^{\mathrm{pr}}(t_i, x) - \rho^-(t_i, x, y)|^2 Q(x, y) \pi(x) \\ &+ \frac{1}{2} \sum_{(x,y) \in \mathcal{X}^2} |\rho^{\mathrm{pr}}(t_i, y) - \rho^+(t_i, x, y)|^2 Q(x, y) \pi(x).\end{aligned}$$

The optimality condition in ρ^{pr} in combination with the reversibility $Q(x, y)\pi(x) = Q(y, x)\pi(y)$ yields for $i = 0, \ldots, N-1$, $x \in \mathcal{X}$

$$\begin{aligned}&\rho^{\mathrm{pr}}(t_i, x) \\ &= \frac{1}{1 + \sum_{y \in \mathcal{X}} Q(x, y)} \left(\rho(t_i, x) + \frac{1}{2} \sum_{y \in \mathcal{X}} (\rho^-(t_i, x, y) + \rho^+(t_i, y, x)) Q(x, y) \right)\end{aligned}$$

and subsequently $\rho^{-\mathrm{pr}}(t_i, x, y) = \rho^{\mathrm{pr}}(t_i, x)$, $\rho^{+\mathrm{pr}}(t_i, x, y) = \rho^{\mathrm{pr}}(t_i, y)$ for $(x, y) \in \mathcal{X} \times \mathcal{X}$. Finally, for $(\rho^{\mathrm{pr}}, \rho^{-\mathrm{pr}}, \rho^{+\mathrm{pr}}) = \mathrm{proj}_{\mathcal{J}_\pm}(\rho, \rho^-, \rho^+)$ using (33) one gets $\mathrm{prox}_{\mathcal{I}^*_{\mathcal{J}_\pm}}(\rho, \rho^-, \rho^+) = (\rho, \rho^-, \rho^+) - (\rho^{\mathrm{pr}}, \rho^{-\mathrm{pr}}, \rho^{+\mathrm{pr}})$.

4.6 Proximal Mapping of $\mathcal{I}^*_{\mathcal{J}_{avg}}$

Once more, we use Moreau's decomposition, (33), to compute the proximal mapping of $\mathcal{I}^*_{\mathcal{J}_{avg}}$ via the projection onto $\mathcal{J}_{avg}$. Note that the original problem (26) does not change if we add the constraint $\rho_h(t_0, \cdot) = \rho_A$ and $\rho_h(t_N, \cdot) = \rho_B$ to the set $\mathcal{J}_{avg}$. That is, we consider the projection onto the set

$$\hat{\mathcal{J}}_{avg} = \left\{(\rho_h, \bar{\rho}_h \in \mathcal{J}_{avg} : \ \rho_h(t_0, \cdot) = \rho_A, \ \rho_h(t_N, \cdot) = \rho_B\right\}.$$

To compute the projection we have to solve

$$\begin{aligned}\operatorname*{arg\,min}_{(\rho_h^{\mathrm{pr}}, \bar{\rho}_h^{\mathrm{pr}}) \in \hat{\mathcal{J}}_{avg}} \ & \frac{1}{2} \sum_{i=0}^{N} \sum_{x \in \mathcal{X}} |\rho_h^{\mathrm{pr}}(t_i, x) - \rho_h(t_i, x)|^2 \pi(x) \\ & + \frac{1}{2} \sum_{i=0}^{N-1} \sum_{x \in \mathcal{X}} |\bar{\rho}_h^{\mathrm{pr}}(t_i, x) - \bar{\rho}_h(t_i, x)|^2 \pi(x).\end{aligned}$$

Thus, we introduce a Lagrange multiplier $\lambda_h \in V^0_{n,h}$ and define the corresponding Lagrangian

$$\begin{aligned}L(\rho_h^{\mathrm{pr}}, \bar{\rho}_h^{\mathrm{pr}}, \lambda_h) = & \frac{1}{2} \sum_{i=0}^{N} \sum_{x \in \mathcal{X}} |\rho_h^{\mathrm{pr}}(t, x) - \rho_h(t, x)|^2 \pi(x) \\ & + \frac{1}{2} \sum_{i=0}^{N-1} \sum_{x \in \mathcal{X}} |\bar{\rho}_h^{\mathrm{pr}}(t, x) - \bar{\rho}_h(t, x)|^2 \pi(x) \\ & - \sum_{i=0}^{N-1} \sum_{x \in \mathcal{X}} \lambda_h(t_i, x) \left(\mathrm{avg}_h \, \rho_h^{\mathrm{pr}}(t_i, x) - \bar{\rho}_h^{\mathrm{pr}}(t_i, x)\right) \pi(x).\end{aligned}$$

We know directly from the added boundary constraints that

$$\rho_h^{\mathrm{pr}}(t_0, x) = \rho_A, \qquad \rho_h^{\mathrm{pr}}(t_N, x) = \rho_B.$$

The optimality condition in ρ_h^{pr} for all $x \in \mathcal{X}$ and for interior time steps $i = 1, \ldots, N-1$ reads as

$$\rho_h^{\mathrm{pr}}(t_i, x) = \rho_h(t_i, x) + \tfrac{1}{2}(\lambda_h(t_{i-1}, x) + \lambda_h(t_i, x)). \tag{34}$$

Further, the optimality condition in $\bar{\rho}_h^{\mathrm{pr}}$ implies that on each interval

$$\bar{\rho}_h^{\mathrm{pr}}(t_i, x) = \bar{\rho}_h(t_i, x) - \lambda_h(t_i, x). \tag{35}$$

Combining both with the constraint $\mathrm{avg}_h\, \rho_h^{\mathrm{pr}}(t_i, x) = \bar{\rho}_h^{\mathrm{pr}}(t_i, x)$, we obtain

$$\begin{aligned}\bar{\rho}_h(t_i, x) - \lambda_h(t_i, x) = \bar{\rho}_h^{\mathrm{pr}}(t_i, x) &= \mathrm{avg}_h\, \rho_h^{\mathrm{pr}}(t_i, x) \\ &= \mathrm{avg}\, \rho_h(t_i, x) + \tfrac{1}{4}(\lambda_h(t_{i-1}, x) + 2\lambda_h(t_i, x) + \lambda_h(t_{i+1}, x))\end{aligned}$$

for all interior elements I_i with $i = 1, \dots, N-2$ and for all $x \in \mathcal{X}$. Analogously, using the boundary conditions we get

$$\begin{aligned}&\bar{\rho}_h(t_0, x) - \lambda_h(t_0, x) = \tfrac{1}{2}(\rho_A(x) + \rho_h(t_1, x)) + \tfrac{1}{4}(\lambda_h(t_0, x) + \lambda_h(t_1, x)) \\ &\bar{\rho}_h(t_{N-1}, x) - \lambda_h(t_{N-1}, x) = \tfrac{1}{2}(\rho_B(x) \\ &\quad + \rho_h(t_{N-1}, x)) + \tfrac{1}{4}(\lambda_h(t_{N-2}, x) + \lambda_h(t_{N-1}, x)).\end{aligned}$$

Thus, for each $x \in \mathcal{X}$ the Lagrange multiplier λ_h satisfies the linear system of equations

$$\begin{aligned}&\tfrac{1}{4}(5\lambda_h(t_0, x) + \lambda_h(t_1, x)) = \bar{\rho}_h(t_0, x) - \tfrac{1}{2}(\rho_A(x) + \rho_h(t_1, x)) \\ &\tfrac{1}{4}(\lambda_h(t_{i-1}, x) + 6\lambda_h(t_i, x) + \lambda_h(t_{i+1}, x)) = \bar{\rho}_h(t_i, x) \\ &\quad - \tfrac{1}{2}(\rho_h(t_{i+1}, x) + \rho_h(t_i, x)) \quad \forall i = 1, \dots, N-2 \\ &\tfrac{1}{4}(\lambda_h(t_{N-2}, x) + 5\lambda_h(t_{N-1}, x)) = \bar{\rho}_h(t_{N-1}, x) - \tfrac{1}{2}(\rho_B(x) + \rho_h(t_{N-1}, x))\end{aligned}$$

This system is solvable, since the corresponding matrix with diagonal $(5, 6, \dots, 6, 5)$ and off-diagonal 1 is strictly diagonal dominant. Then, given the Lagrange multiplier λ_h, the solution of the projection problem is given by (34) and (35). Finally, the proximal map of $\mathcal{I}^*_{\mathcal{J}_{avg}}$ can be computed by Moreau's identity, (33). Thus, to compute the proximal mapping of $\mathcal{I}^*_{\hat{\mathcal{J}}_{avg}}$ one must solve a sparse system in time for each graph node separately. Since the involved matrix is constant, it can be pre-factored.

4.7 Proximal Mapping of $\mathcal{I}_{\mathcal{J}_=}$

The proximal map of $\mathcal{I}_{\mathcal{J}_=}$ is given by the projection

$$\begin{aligned}\mathrm{proj}_{\mathcal{J}_=}(\bar{\rho}_h, q_h) = &\operatorname*{arg\,min}_{(\bar{\rho}_h^{\mathrm{pr}}, q_h^{\mathrm{pr}}) \in V^0_{n,h} \times V^0_{n,h} \,:\, \bar{\rho}_h^{\mathrm{pr}} = q_h^{\mathrm{pr}}} \\ &\frac{1}{2} h \sum_{i=0}^{N-1} \sum_{x \in \mathcal{X}} \left(|\bar{\rho}_h - \bar{\rho}_h^{\mathrm{pr}}|^2 + |q_h - q_h^{\mathrm{pr}}|^2 \right) \pi(x) \\ &= \frac{1}{2}(\bar{\rho}_h + q_h, \bar{\rho}_h + q_h).\end{aligned}$$

5 Numerical results

In what follows we compare the numerical solution based on our discretization with the explicitly known solution for a simple model with just two nodes. Furthermore, we apply our method to a set of characteristic test cases to study the qualitative and quantitative behaviour of the discrete transportation distance.

Comparison with the exact solution for the 2-node case Consider a two point graph $\mathcal{X} = \{a, b\}$ with Markov chain and stationary distribution

$$Q = \begin{pmatrix} 0 & p \\ q & 0 \end{pmatrix}, \quad \pi = \begin{pmatrix} \frac{q}{p+q} \\ \frac{p}{p+q} \end{pmatrix},$$

where $p, q \in (0, 1]$. For this case, Maas [16] constructed an explicit solution for the geodesic from $\rho_A = \left(\frac{p+q}{q}, 0\right)$ to $\rho_B = \left(0, \frac{p+q}{p}\right)$. Note that every probability measures on $\mathcal{X}$ can be described by a single parameter $r \in [-1, 1]$ via

$$\rho(r) = (\rho_a(r), \rho_b(r)) = \left(\frac{p+q}{q}\frac{1-r}{2}, \frac{p+q}{p}\frac{1+r}{2}\right).$$

Especially, we have $\rho_A = \rho(-1)$ and $\rho_B = \rho(1)$. Using this representation, Maas showed that for $-1 \leq \alpha \leq \beta \leq 1$ the optimal transport distance is given by

$$\mathcal{W}(\rho(\alpha), \rho(\beta)) = \frac{1}{2}\sqrt{\frac{1}{p} + \frac{1}{q}} \int_\alpha^\beta \frac{1}{\sqrt{\theta(\rho_a(r), \rho_b(r))}}\, \mathrm{d}r \tag{36}$$

and the optimal transport geodesic from $\rho(\alpha)$ to $\rho(\beta)$ is given by $\rho(\gamma(t))$ for $t \in [0, 1]$, where γ satisfies the differential equation

$$\gamma'(t) = 2(\beta - \alpha)\mathcal{W}(\rho(\alpha), \rho(\beta))\sqrt{\frac{pq}{p+q}\theta(\rho(\gamma_a(t)), \rho_b(\gamma(t))}. \tag{37}$$

For the special case, where θ is the logarithmic mean $\theta_{\log}$ and $p = q$, one obtains that $\theta_{\log}(\rho_a(r), \rho_b(r)) = \frac{r}{\operatorname{arctanh}(r)}$. and consequently the discrete transport distance is given by $\mathcal{W}(\rho(\alpha), \rho(\beta)) = \frac{1}{\sqrt{2p}} \int_\alpha^\beta \sqrt{\frac{\operatorname{arctanh}(r)}{r}}\, \mathrm{d}r$. Furthermore, the optimal transport geodesic from $\rho(\alpha)$ to $\rho(\beta)$ is given by $\rho(\gamma(t))$ for $t \in [0, 1]$, where γ satisfies the differential equation $\gamma'(t) = \sqrt{2p}(\beta - \alpha)\mathcal{W}(\rho(\alpha), \rho(\beta))\sqrt{\frac{\gamma(t)}{\operatorname{arctanh}(\gamma(t))}}$. For this two point graph we numerically compute the optimal transport geodesic. This allows us to evaluate directly the distance $\mathcal{W}$, which we can compare with a numerical quadrature of (36). Using the approximation of $\mathcal{W}$, we use an explicit Euler scheme to compute the solution ρ_h^{ODE} of the ODE (37). For the case $p = q = 1$ we compare our numerical solution to the Euler approximation for the ODE for $N = 2000$ in Fig. 4.

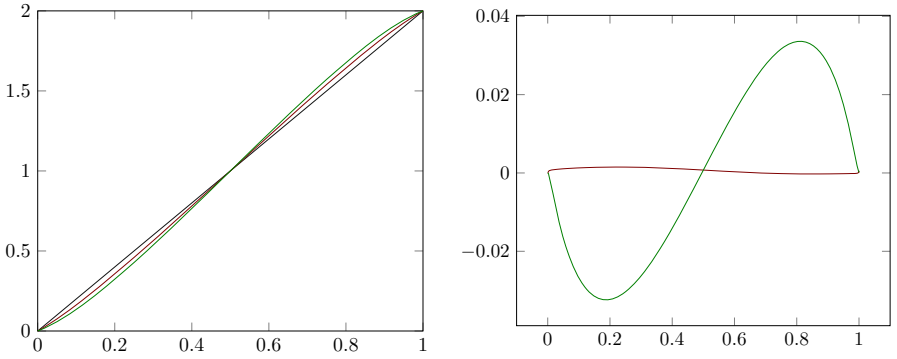

Fig. 4 The mass distribution at b is plotted over time $t \in [0, 1]$. Left: numerical solution for a 2-point graph $\mathcal{X} = \{a, b\}$ for the logarithmic (red) and geometric (green). The black line represents the diagonal, which is the solution in the case of the (non admissible) arithmetic averaging. Right: Difference of the numerical solution for the logarithmic (red) and geometric (green) mean with the Euler scheme solution ρ_h^{ODE} for the logarithmic mean (color figure online)

Geodesics on some selected graphs In the following we study the behavior of the discrete optimal transport distance on some simple graphs. If $G = (\mathcal{X}, E)$ is an undirected graph with vertex set $\mathcal{X}$ and edge set E, we usually set the stationary distribution and the Markov kernel to

$$\pi(x) = \frac{d(x)}{|E|}, \quad Q(x, y) = \begin{cases} \frac{1}{\pi(x)|E|}, & (x, y) \in E, \\ 0, & \text{else}, \end{cases} \tag{38}$$

where for each node x we denote by $d(x)$ the number of outgoing edges. The underlying time step size is $h = \frac{1}{100}$. The solution (ρ, m) is displayed at intermediate time steps indicated on the arrow in the first row. For each of these time steps, blue discs and red arrows superimposed over the graph display mass and momentum at nodes and on edges, respectively. The area of a disc is proportional to the mass $\rho(x)\pi(x)$. A red arrow connecting nodes x and y renders the momentum $m(x, y)$. The direction of the arrow indicates the direction of the flow, i.e. it points from x to y if $m(y, x) = -m(x, y) > 0$ (cf. Lemma 2.4). The thickness of an arrow is proportional to $|m(x, y)|Q(x, y)\pi(x)$. Underneath these graph drawings both, mass and the momentum on nodes and edges, are plotted in histograms. The plots associated with $t = 0$ and $t = 1$ show the prescribed boundary conditions in time. As the stopping criteria for the iterative algorithm in (28) we choose $\int_0^1 \|\rho^{k+1} - \rho^k\|_\pi^2 \, \mathrm{d}t$ with threshold 10^{-10}, where k denotes the iteration step.

First, we consider in Fig. 5 numerically computed geodesic paths on circles with three and four nodes, where the initial mass ρ_A is supported on a single node x and the mass ρ_B is supported on a single neighboring node of x (see also the motivating Fig. 2). We observe that in the case of three points a small amount of mass is also transport along the longer path, whereas for a circle with four nodes all mass is transported along the shortest connecting path.

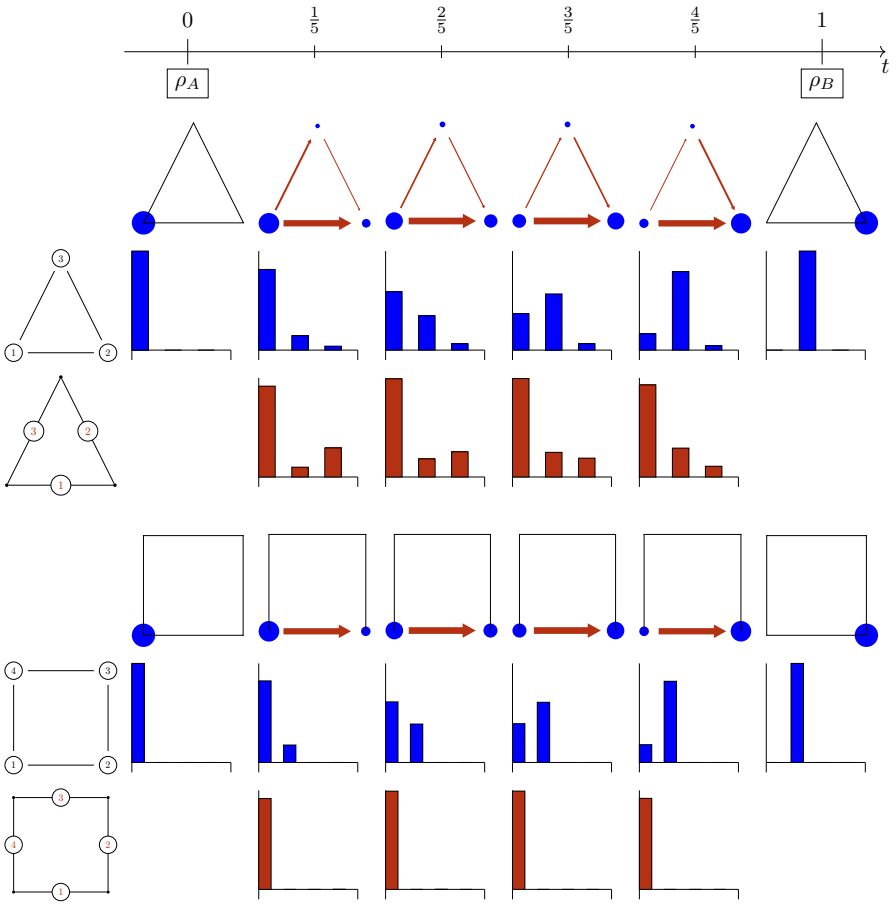

Fig. 5 Numerically computed geodesics on circles with three and four nodes and corresponding histograms of the mass and momentum variable

Next, we investigate in Fig. 6 the diffuse behavior on a 3×3 lattice by transporting mass from the middle left to the middle right. Since the 3×3 lattice consists of subgraphs given by circles with four nodes, we would expect that also on the lattice mass is only transported along the shortest path. Indeed, it has been recently established in [11] that a so-called retraction property on a subgraph is sufficient to guarantee that geodesics are supported on this subgraph. For $Q = 1$ and $\pi = 1$ the retraction property can be verified for the middle horizontal line and thus mass is only transport along this shortest path. However, for Q and π chosen as in (38), the retraction property does not hold and our numerical results show that an essential amount of mass is not transported along the middle horizontal line.

Figure 7 visualizes in the same fashion an optimal transport path on the graphs of the cube and of the hypercube. Note that for the computed solutions are symmetric. In explicit, mass and momentum at time t equal the mass and the momentum at time $1 - t$ on point reflected nodes and edges, respectively. Furthermore, the distribution

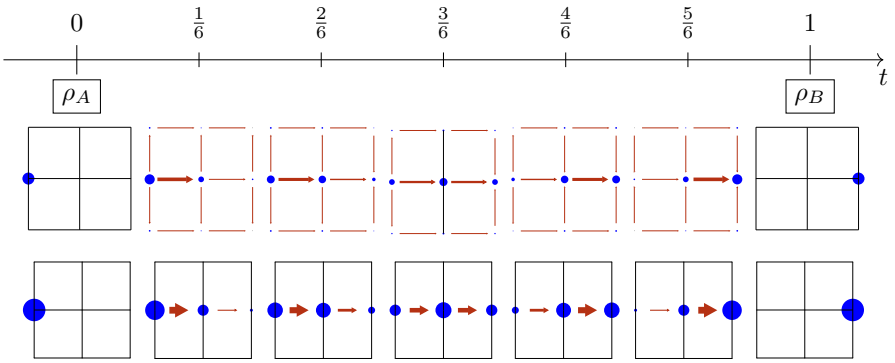

Fig. 6 Numerically computed geodesics on a 3×3 lattice for different choices of Q and π. Top: Markov kernel Q and stationary distribution π given as in (38). Bottom: $Q(x, y) = 1$ for all edges (x, y) and $\pi(x) = 1$ for all nodes x

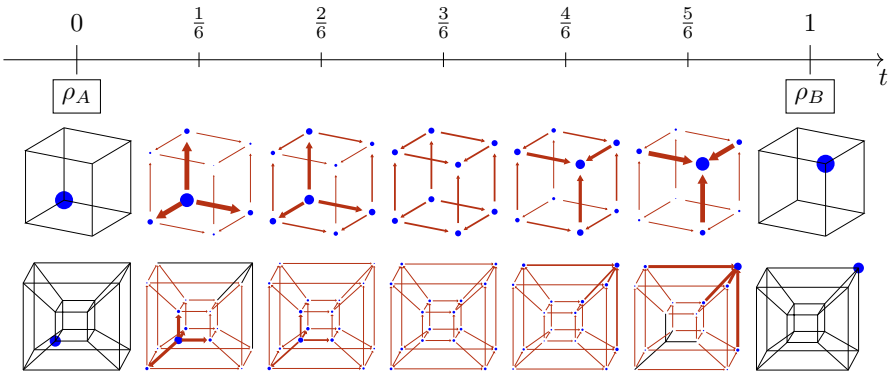

Fig. 7 Numerically computed geodesic on the cube (top) and the hypercube (bottom). We observe an equidistribution of the mass at time $t = \frac{1}{2}$

of mass is constant on all nodes at time $t = \frac{1}{2}$. Finally, in Fig. 8 we depict an example of a graph with four nodes, which shows that the sign of the momentum variable on a fixed edge may change along a geodesic path.

Convergence in time In Theorem 3.8 we have established convergence of minimizing paths of our fully discrete approximation for a time step size $h \to 0$. Now, we study this convergence numerically. We consider a square lattice with 3×3 nodes and compute an optimal transport path between the mass $\rho_A = \delta_{(\frac{1}{2},\frac{1}{2})}$ concentrated at the midpoint of the square and a uniform mass distribution $\rho_B = \mathbb{1}$. For the discretization in time we choose step sizes $N = 8, 16, 32, 64, 128, 256, 512$. Since we do not know the exact solution for this example, we use as a substitute the numerical result $(\rho_{\text{approx}}, m_{\text{approx}})$ for the finest discretization $N = 1024$ to which we compare when computing numerical errors. We study approximation errors for mass and momentum in the same norms for which we have shown convergence in the numerical analysis. More precisely, we use $\|\rho_{\text{approx}} - \rho_h\|_{H^1([0,1],\mathbb{R}^{\mathcal{X}})}$ and $\|m_{\text{approx}} - m_h\|_{L^2([0,1],\mathbb{R}^{\mathcal{X}})}$.

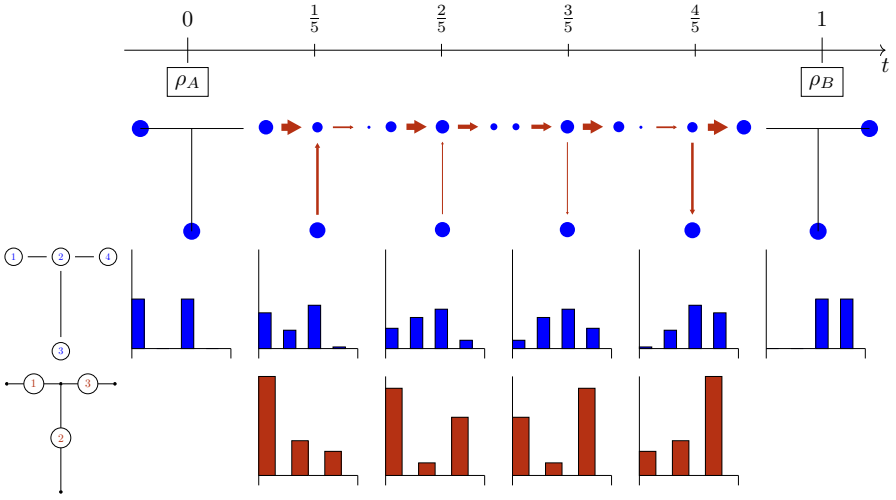

Fig. 8 Numerically computed geodesic on a graph with four nodes. Note that the sign of m for edge 2 changes (cf. $t = \frac{1}{5}$ and $t = \frac{4}{5}$)

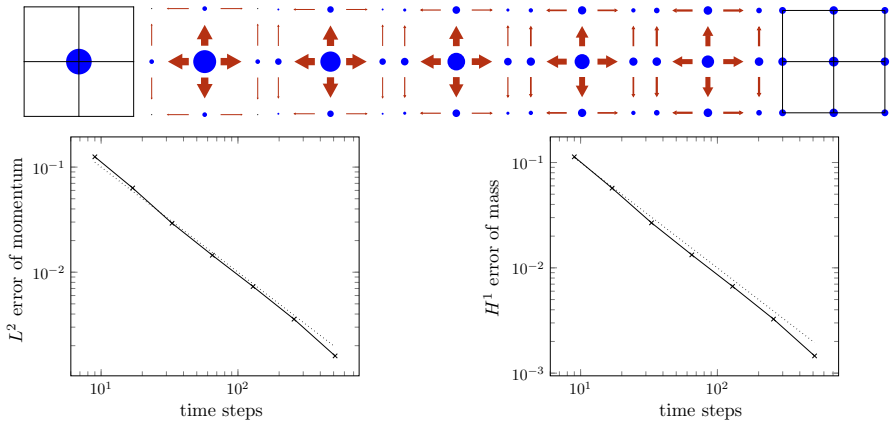

Fig. 9 Numerical verification of the convergence in time for step sizes $N = 8, 16, 32, 64, 128, 256, 512, 1024$ for a square lattice of 3×3 nodes. Below we plot the errors $\|m_{\text{approx}} - m_h\|_{L^2([0,1],\mathbb{R}^{\mathcal{X}})}$ and $\|\rho_{\text{approx}} - \rho_h\|_{H^1([0,1],\mathbb{R}^{\mathcal{X}})}$ in a log-log scale. The convergence order is linear in h (dotted lines)

In Fig. 9 we plot these errors in a log-log diagram and experimentally obtain linear convergence in h.

Experimental results related to the Gromov–Hausdorff convergence for simple graphs In [14] it was shown that for the d-dimensional torus $\mathbf{T}^d$ the discrete transportation distance $\mathcal{W}$ on a discretized torus $\mathbf{T}^d_M$ with uniform mesh size $\frac{1}{M}$ converges in the Gromov–Hausdorff metric to the classical L^2-Wasserstein distance on $\mathbf{T}^d$. In fact, the optimal transport with respect to the classical L^2-Wasserstein distance between two point masses is a point mass traveling along the connecting straight line.

Concerning the expected concentration of the transport along this line we perform the following numerical experiments for $d = 1, 2$. We first consider for $d = 1$ the unit interval $I = [0, 1]$ and a sequence of space discretizations $\mathcal{X}_M = \{x_0, \dots, x_M\}$ with uniform mesh size $\frac{1}{M}$ with $M \in \mathbb{N}$. The corresponding Markov kernel Q_M for $\mathcal{X}_M$ is defined by $Q_M(x_i, x_{i+1}) = Q_M(x_i, x_{i-1}) = \frac{1}{2}$ for $i = 1, \dots, x_{M-1}$ and $Q_M(x_0, x_1) = 1 = Q_M(x_M, x_{M-1})$. The continuous L^2-Wasserstein geodesic connecting $\rho_A = \delta_0$ and $\rho_B = \delta_1$ is given by the transport of the Dirac measure with constant speed:

$$\rho(t, x) = \delta_t(x).$$

In Fig. 10 we plot the density distribution of the discrete optimal transport geodesic at time $t = \frac{1}{2}$ for different grid sizes $\frac{1}{M}$. One observes the onset of mass concentration in space at that time at the location $x = \frac{1}{2}$ for increasing M. To quantify the Gromov–Hausdorff convergence, we compute the L^2-Wasserstein distance of the approximatively computed discrete geodesic at time $t = \frac{1}{2}$ to the Dirac measure $\delta_{\frac{1}{2}}$, which is explicitly given by

$$W_2\left(\rho_M\left(\tfrac{1}{2}\right), \delta_{\frac{1}{2}}\right)^2 = \sum_{m=0}^{M} \left|\tfrac{m}{M} - \tfrac{1}{2}\right|^2 \rho_M\left(\tfrac{1}{2}, \tfrac{m}{M}\right).$$

In Table 1 we compute the expected order of convergence. As an initialization of the variables in the proximal splitting algorithm we use an adaptive scheme in time, i.e. we first compute a solution for $N = 32$, then prolongate this result to a finer discretization by doubling N and repeat until $N = 1024$. The log-log plot in Fig. 10 shows a convergence order $\frac{1}{2}$ in the L^2-Wasserstein distance with respect to the associated space discretization width. Moreover, one observes that the discrete optimal transport of a Dirac measure behaves fairly singular. In fact, one frequently has to deal with the projection onto 0 on the cone K. To quantify the error due to the space discretization, this error has to dominate the time discretization error with its linear convergence of the mass and momentum variable in the appropriate norms. Indeed, for $M = 256$ the time discretization error seems to be still comparably large for $N = 1024$ indicated by slight flattening of the curve on the right.

For $d = 2$ we consider a square lattice of uniform grid size $\frac{1}{M}$ with $M \in \mathbb{N}$ and nodes $\mathcal{X}_M = \{(i/M, j/M) : i, j \in (0, \dots, M)\}$. The weights of the Markov kernel Q are proportional to the number of adjacent edges. Now, we investigate a discrete geodesic connecting the Dirac masses $\delta_{(0,0)}$ and $\delta_{(1,1)}$. An example for $M = 2$ is depicted in Fig. 11. One expects that for increasing M mass on bands parallel to the space diagonal will decrease. In Fig. 12 we plot for decreasing mesh size $\frac{1}{M}$ the in time accumulated density values along the diagonal and the off-diagonals bands of nodes. More precisely, we define the bands of nodes $l_M^i = \{(x_1, x_2) \in \mathcal{X}_M \times \mathcal{X}_M : x_2 = x_1 + \frac{i}{M}\}$ ($i = 0$ being the diagonal) and compare the values $\int_0^1 \sum_{x \in l_M^i} \rho(t, x)\pi(x)\, \mathrm{d}t$.

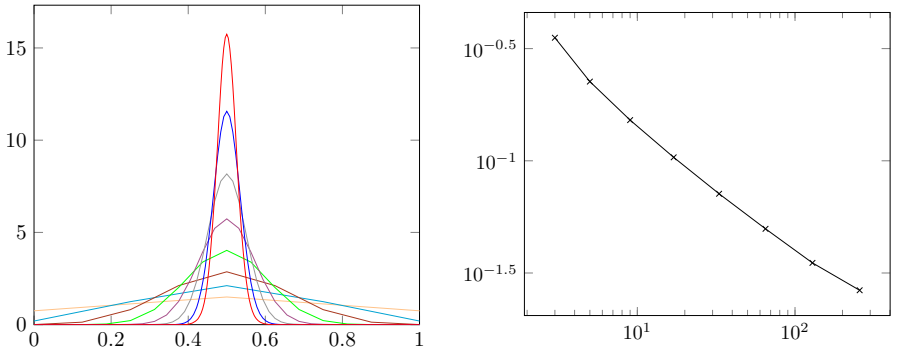

Fig. 10 Left: linearly interpolated densities for the $\mathcal{W}$ geodesic on a one dimensional chain graph with M nodes between a Dirac mass at the beginning and the end, at $t = 0.5$ with $M = 2$ (yellow), 4 (turquoise), 8 (brown), 16 (green), 32 (violet), 64 (gray), 128 (blue), and 256 (red). Right: Convergence of the L^2-Wasserstein geodesic to a Dirac measure at $x = \frac{1}{2}$ for increasing M (color figure online)

Table 1 Expected order of convergence of the discrete geodesics from Fig. 10 in the L^2-Wasserstein distance

M	$\mathcal{W}_M := W_2\left(\rho_M\left(\frac{1}{2}\right), \delta_{\frac{1}{2}}\right)$	EOC $= \frac{\log(\mathcal{W}_M/\mathcal{W}_{M/2})}{\log(1/2)}$
2	0.3535819979	
4	0.225432747	0.649347723
8	0.1518529497	0.5700221686
16	0.1036187107	0.5513903948
32	0.071299038	0.5393300146
64	0.0497631136	0.5188058612
128	0.0350786465	0.5044836728
256	0.0264826129	0.4055476142

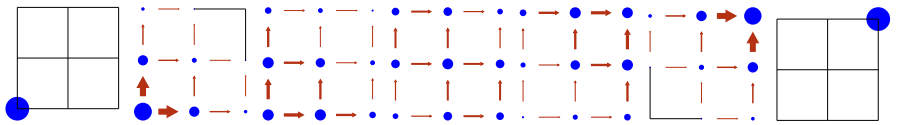

Fig. 11 Numerically computed geodesics on a 3×3 lattice connecting $\rho_A = \delta_{(0,0)}$ and $\rho_B = \delta_{(1,1)}$

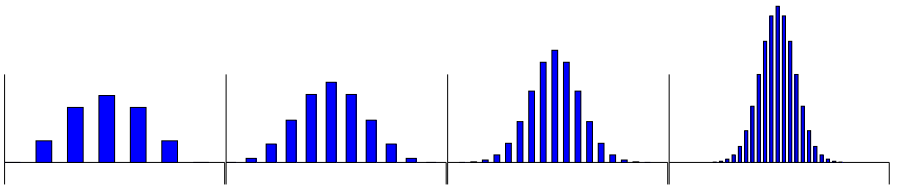

Fig. 12 Geodesics in the distance $\mathcal{W}$ on a two dimensional grid graph between Dirac masses at diagonally opposite ends. We show accumulated densities along the diagonal and the off-diagonals (see text for details). From left to right: $M = 4, 8, 16, 32$. The width of the bars is scaled with the number of lines

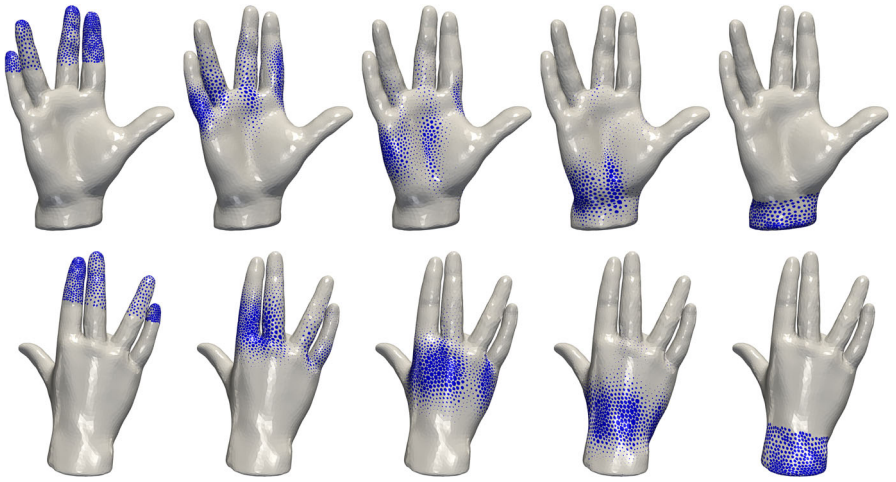

Fig. 13 Extraction of a discrete optimal transport geodesic for a triangular mesh of a human hand with 6094 vertices. First and second row provide visualizations from two different perspectives. The geodesic is computed based on 33 time steps and we depict the result at time steps $t = 0, 9, 17, 25, 33$. For each vertex we represent the mass by a blue neighborhood with an area proportional to the mass

Discrete geodesic on a triangular mesh of a human hand In Fig. 13 we consider a significantly more complex discrete graph, given by a triangular mesh of a human hand and compute the discrete optimal transport geodesic between a mass ρ_A supported on the fingers and a mass ρ_B supported on the wrist to demonstrate the robustness of our approach also for larger graphs.

6 Simulation of the gradient flow of the entropy

The entropy functional on $\mathcal{P}(\mathcal{X})$ is given by

$$\mathcal{H}(\rho) = \sum_{x \in \mathcal{X}} \rho(x) \log(\rho(x)) \pi(x).$$

with the usual convention '$0 \log 0 = 0$'. Maas [16] proved that for the logarithmic mean $\theta_{\log}(\cdot, \cdot)$ and $\rho \in \mathcal{P}(\mathcal{X})$ the heat flow $t \mapsto e^{t\Delta_{\mathcal{X}}} \rho$ is a gradient flow trajectory for the entropy $\mathcal{H}(\rho)$ with respect to the discrete transportation distance $\mathcal{W}$. In [10] it was shown that a similar result holds true for the Renyi entropy

$$\mathcal{H}_m(\rho) = \frac{1}{m-1} \sum_{x \in \mathcal{X}} \rho(x)^m \pi(x).$$

In fact, for $m = \frac{1}{2}$ and the gradient flow of $\mathcal{H}_m$ with respect to the metric $\mathcal{W}$ constructed with θ being the geometric mean $\theta_{\text{geom}}(\cdot, \cdot)$ is given by the porous medium equation $\partial_t \rho = \Delta_{\mathcal{X}} \rho^m$.

To test the correctness of our numerical method, we compute the gradient flow of the entropy w.r.t. the dicrete optimal transport distance $\mathcal{W}$ numerically and compare it to standard numerical solutions to the discrete heat and porous medium equations. To this end, we consider a line of five points with stationary distribution $\pi = \frac{1}{5}(1, 2, 2, 2, 1)$, Markov kernel $Q(x, y) = \frac{1}{10\pi(x)}$ for x, y adjacent, and initial mass $\rho = \frac{1}{10}(1, 1, 5, 1, 1)$. Following [1,15], for an initial density $\rho_0 \in \mathcal{P}(\mathcal{X})$ and a time step size $\tau > 0$ an implicit time-discrete gradient flow scheme for $\mathcal{H}$ can be defined by

$$\rho_{k+1} = \arg\min_{\rho_B} \frac{1}{2}\mathcal{W}_h(\rho_k, \rho_B)^2 + \tau \cdot \mathcal{H}(\rho_B) \tag{39}$$

with an inner time step size h appearing in the discretization $\mathcal{W}_h$ of $\mathcal{W}$. To minimize this functional numerically, we simultaneously carry out the external optimization over ρ and the internal optimization within $\mathcal{W}_h$. To this end, we define a discrete continuity equation with one free endpoint. For initial datum $\rho_A \in \mathcal{P}(\mathcal{X})$ let

$$\mathcal{CE}_h(\rho_A) = \left\{(\rho_h, m_h, \rho_B) \in V^1_{n,h} \times V^0_{e,h} \times \mathbb{R}^{\mathcal{X}} \,:\, (\rho_h, m_h) \in \mathcal{CE}_h(\rho_A, \rho_B)\right\}.$$

Analogous to (26), problem (39) can be written as

$$\begin{aligned}\min \{&\mathcal{F}(\rho_h, m_h, \vartheta_h, \rho_h^-, \rho_h^+, \bar\rho_h, q_h, \rho_B) + \mathcal{G}(\rho_h, m_h, \vartheta_h, \rho_h^-, \rho_h^+, \bar\rho_h, q_h, \rho_B) \,:\\ &(\rho_h, m_h, \vartheta_h, \rho_h^-, \rho_h^+, \bar\rho_h, q_h, \rho_B) \in V^1_{n,h} \times (V^0_{e,h})^4 \times (V^0_{n,h})^2 \times \mathbb{R}^{\mathcal{X}}\}\end{aligned}$$

with

$$\begin{aligned}&\mathcal{F}(\rho_h, m_h, \vartheta_h, \rho_h^-, \rho_h^+, \bar\rho_h, q_h, \rho_B) := \widehat{\mathcal{A}}(\vartheta_h, m_h)\\ &\quad + \mathcal{I}_{\mathcal{J}_\pm}(q_h, \rho_h^-, \rho_h^+) + \mathcal{I}_{\mathcal{J}_{avg}}(\rho_h, \bar\rho_h) + 2\,\tau \cdot \mathcal{H}(\rho_B)\,,\\ &\mathcal{G}(\rho_h, m_h, \vartheta_h, \rho_h^-, \rho_h^+, \bar\rho_h, q_h, \rho_B) := \mathcal{I}_{\mathcal{CE}_h(\rho_k)}(\rho_h, m_h, \rho_B) + \mathcal{I}_{\mathcal{K}}(\rho_h^-, \rho_h^+, \vartheta_h)\\ &\quad + \mathcal{I}_{\mathcal{J}_=}(\bar\rho_h, q_h).\end{aligned}$$

Again, this is amenable for algorithm (28). We extend the space H by a factor $\mathbb{R}^{\mathcal{X}}$ and adapt the scalar product on H (27) adding the term $h\,\langle\rho_{B,1}(\cdot), \rho_{B,2}(\cdot)\rangle_\pi$ with respect or the additional variable ρ_B. The proximal step of $\mathcal{F}^*$ then entails an additional proximal step of $(2\,\tau \cdot \mathcal{H})^*$ with respect to $h\|\cdot\|_\pi$ and in the proximal step of G the projection onto $\mathcal{CE}_h(\rho_A, \rho_B)$ is replaced by a projection onto $\mathcal{CE}_h(\rho_k)$. Next, we detail these modifications.

Let us recall that the proximal mapping of $(\gamma \cdot \mathcal{H})^*$ and $\gamma \cdot \mathcal{H}$ are linked by Moreau's decomposition, cf. (33). The computation of the the proximal mapping for $\gamma \cdot \mathcal{H}$ decouples in space and the resulting one dimensional problem can be solved via Newton's method. This decoupling is possible since we do not enforce the constraint $\rho_B \in \mathcal{P}(\mathcal{X})$ in the formulation of $\mathcal{H}$ but enforce it via the discrete continuity equation constraint.

To implement the projection

$$\begin{aligned}\mathrm{proj}_{\mathcal{CE}_h(\rho_A)}(\rho, m, \rho_B) = &\operatorname*{arg\,min}_{(\rho^{\mathrm{pr}}, m^{\mathrm{pr}}, \rho_B^{\mathrm{pr}}) \in \mathcal{CE}_h(\rho_A)} \frac{h}{2} \sum_{i=0}^{N} \|\rho_h^{\mathrm{pr}}(t_i, \cdot) - \rho_h(t_i, \cdot)\|_\pi^2 \\ &+ \frac{h}{2} \sum_{i=0}^{N-1} \|m_h^{\mathrm{pr}}(t_i, \cdot) - m_h(t_i, \cdot)\|_Q^2 + \frac{h}{2} \|\rho_B^{\mathrm{pr}} - \rho_B\|_\pi^2 \end{aligned} \tag{40}$$

onto the set $\mathcal{CE}_h(\rho_A)$ of solutions of the discrete continuity equation with initial data ρ_A the following modifications apply. Analogous to Proposition 4.3, a space time discrete elliptic equation

$$\begin{aligned}&\frac{\varphi_h(t_1, x) - \varphi_h(t_0, x)}{h^2} + \triangle_{\mathcal{X}} \varphi_h(t_0, x) = -\left(\frac{\rho_h(t_1, x) - \rho_A(x)}{h} + \mathrm{div} m_h(t_0, x) \right), \\ &\frac{-\frac{3}{2}\varphi_h(t_{N-1}, x) - \varphi_h(t_{N-2}, x)}{h^2} + \triangle_{\mathcal{X}} \varphi_h(t_{N-1}, x) \\ &= -\left(\frac{\frac{1}{2}(\rho_B(x) + \rho_h(t_N, x)) - \rho_h(t_{N-1}, x)}{h} + \mathrm{div} m_h(t_{N-1}, x) \right), \\ &\frac{\varphi_h(t_{i+1}, x) - 2\varphi_h(t_i, x) + \varphi_h(t_{i-1}, x)}{h^2} + \triangle_{\mathcal{X}} \varphi_h(t_i, x) \\ &= -\left(\frac{\rho_h(t_{i+1}, x) - \rho_h(t_i, x)}{h} + \mathrm{div} m_h(t_i, x) \right)\end{aligned}$$

with $i = 1, \ldots, N-2$ and $x \in \mathcal{X}$ has to be solved for the Lagrange multiplier $\varphi_h \in V_{n,h}^0$. Note that this system is no longer degenerate due to the additional freedom of ρ_B and thus no regularization as before is required. Then the solution $(\rho^{\mathrm{pr}}, m^{\mathrm{pr}}, \rho_B^{\mathrm{pr}})$ to (40) is given by

$$\begin{aligned}\rho_B^{\mathrm{pr}}(x) &= \frac{1}{2}\left(\rho_h(t_N, x) + \rho_B(x) - \frac{\varphi_h(t_{N-1}, x)}{h} \right), \\ \rho_h^{\mathrm{pr}}(t_i, x) &= \rho_h(t_i, x) + \frac{\varphi_h(t_i, x) - \varphi_h(t_{i-1}, x)}{h}, \\ \rho_h^{\mathrm{pr}}(t_0, x) &= \rho_A(x), \ \rho_h^{\mathrm{pr}}(t_N, x) = \rho_B^{\mathrm{pr}}(x), \\ m_h^{\mathrm{pr}}(t_i, x, y) &= m_h(t_i, x, y) + \nabla_{\mathcal{X}} \varphi_h(t_i, x, y)\end{aligned}$$

for all $i = 1, \ldots, N-2$ and $x, y \in \mathcal{X}$. In Fig. 14 we compare the numerical results for this natural discretization of the gradient flow of the entropy to the flow computed numerically with a simple explicit Euler discretization applied to the heat equation and the porous medium equation, respectively, with respect to the underlying Markov kernel.

Note that the entropy functional $\mathcal{H}$ is minimized for equidistributed $\rho \in \mathcal{P}(\mathcal{X})$. Thus, in the example above we expect that the iterates ρ_k in (39) converge to the uniform distribution $\mathbb{I} = (1, 1, 1, 1, 1)$ for $k \to \infty$ which is confirmed numerically. In

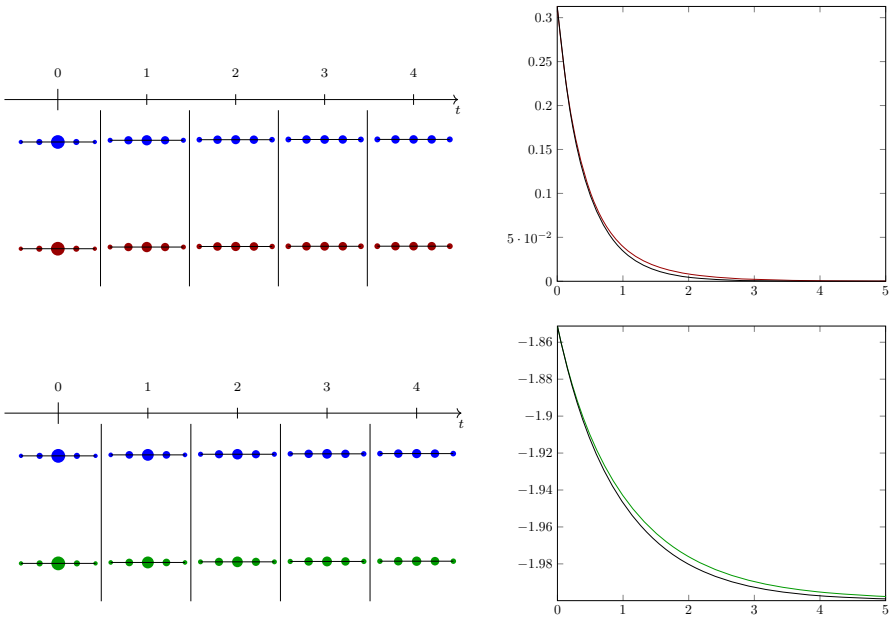

Fig. 14 Numerical solution of the heat flow (top) and the porous medium equation (bottom) based on an explicit Euler scheme (blue) with time step size 10^{-3} and for the gradient flow of the associated entropy using the logarithmic mean (red) and the geometric mean (green), respectively, with $\tau = 10^{-3}$ and $h = 100$. Panels on the left show the mass distributions on the graph at different times, panels on the right show the values of the entropies over time (color figure online)

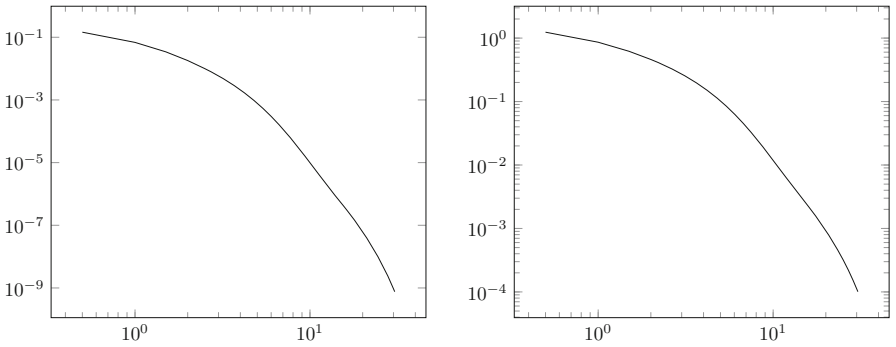

Fig. 15 Convergence of gradient flow of the entropy using the logarithmic mean. We use a time step size $\tau = 10^{-3}$, $h = 100$ and $3 \cdot 10^4$ minimizing movement steps. Left: entropy functional $\mathcal{H}(\rho_k)$. Right: Difference to the uniform distribution $\|\rho_k - \mathbb{I}\|_2$

Fig. 15 we plot for $3 \cdot 10^4$ minimizing movement steps the entropy functional $\mathcal{H}(\rho_k)$ and the difference to the uniform distribution $\|\rho_k - \mathbb{I}\|_2$ in a log-scale. We observe in both cases an exponential decay rate.

References

1. Ambrosio, L., Gigli, N., Savaré, G.: Gradient flows: in metric spaces and in the space of probability measures. Springer, Berlin (2008)
2. Ahuja, R.K., Magnanti, T.L., Orlin, J.B.: Network Flows: Theory, Algorithms, and Applications. Prentice-Hall Inc, Englewood Cliffs (1993)
3. Benamou, J.-D., Brenier, Y.: A computational fluid mechanics solution to the Monge–Kantorovich mass transfer problem. Numer. Math. **84**(3), 375–393 (2000)
4. Bauschke, H.H., Combettes, P.L.: Convex Analysis and Monotone Operator Theory in Hilbert Spaces. CMS Books in Mathematics, 1st edn. Springer, Berlin (2011)
5. Chow, S.-N., Huang, W., Li, Y., Zhou, H.: Fokker-planck equations for a free energy functional or markov process on a graph. Arch. Ration. Mech. Anal. **203**(3), 969–1008 (2012)
6. Carrillo, J.A., Jüngel, A., Santos, M.C.: Displacement convexity for the entropy in semi-discrete non-linear fokker-planck equations. Eur. J. Appl. Math. **1–20**, (2018). https://doi.org/10.1017/S0956792517000389
7. Chambolle, A., Pock, T.: A first-order primal-dual algorithm for convex problems with applications to imaging. J. Math. Imaging Vis. **40**(1), 120–145 (2011)
8. Disser, K., Liero, M.: On gradient structures for Markov chains and the passage to Wasserstein gradient flows. Netw. Heterog. Media **10**(2), 233–253 (2015)
9. Erbar, M., Maas, J.: Ricci curvature of finite Markov chains via convexity of the entropy. Arch Ration. Mech. Anal. **206**(3), 997–1038 (2012)
10. Erbar, M., Maas, J.: Gradient flow structures for discrete porous medium equations. Discrete Contin. Dyn. Syst. **34**(4), 1355–1374 (2014)
11. Erbar, M., Maas, J., Wirth, M.: On the geometry of geodesics in discrete optimal transport. Calc. Var. Partial Differ. Eq., **58**(1):Art. 19, 19 (2019)
12. Essid, M., Solomon, J.: Quadratically regularized optimal transport on graphs. SIAM J. Sci. Comput. **40**(4), A1961–A1986 (2018)
13. Gladbach, P., Kopfer, E., Maas, J.: Scaling limits of discrete optimal transport. arxiv:1809.01092 (2018)
14. Gigli, N., Maas, J.: Gromov–Hausdorff convergence of discrete transportation metrics. SIAM J. Math. Anal. **45**(2), 879–899 (2013)
15. Jordan, R., Kinderlehrer, D., Otto, F.: The variational formulation of the Fokker–Planck equation. SIAM J. Math. Anal. **29**(1), 1–17 (1998)
16. Maas, J.: Gradient flows of the entropy for finite Markov chains. J. Funct. Anal. **261**(8), 2250–2292 (2011)
17. McCann, R.J.: A convexity principle for interacting gases. Adv. Math. **128**(1), 153–179 (1997)
18. Mielke, A.: A gradient structure for reaction–diffusion systems and for energy-drift-diffusion systems. Nonlinearity **24**(4), 1329 (2011)
19. Mielke, A.: Geodesic convexity of the relative entropy in reversible Markov chains. Calc. Var. Partial Differ. Equ. **48**, 1–31 (2013)
20. Otto, F.: The geometry of dissipative evolution equations: the porous medium equation. Commun. Partial Differ. Equ. **26**(1–2), 101–174 (2001)
21. Papadakis, N., Peyré, G., Oudet, E.: Optimal transport with proximal splitting. SIAM J. Imaging Sci. **7**(1), 212–238 (2014)
22. Santambrogio, F.: Optimal Transport for Applied Mathematicians, vol. 87 of Progress in Nonlinear Differential Equations and Their Applications. Birkhäuser Boston (2015)
23. Solomon, J., Rustamov, R., Guibas, L., Butscher, A.: Earth mover's distances on discrete surfaces. In: ACM Transactions on Graphics (Proc. of SIGGRAPH 2014), 33(4) (2014)
24. Solomon, J., Rustamov, R., Guibas, L., Butscher, A.: Continuous-flow graph transportation distances. arXiv:1603.06927 (2016)
25. Villani, C.: Optimal Transport: Old and New, volume 338 of Grundlehren der mathematischen Wissenschaften. Springer, Berlin (2009)